Meteoritics & Planetary Science 41, Nr 3, 433–454 (2006)
Abstract available online at http://meteoritics.org

Shock-metamorphosed zircon in terrestrial impact craters

A. WITTMANN*, T. KENKMANN, R. T. SCHMITT, and D. STÖFFLER

Institut für Mineralogie, Museum für Naturkunde, Humboldt Universität zu Berlin, Invalidenstrasse 43, 10115 Berlin, Germany
*Corresponding author. E-mail: axel.wittmann@museum.hu-berlin.de

(Received 06 June 2005; revision accepted 11 October 2005)

Abstract–To ascertain the progressive stages of shock metamorphism of zircon, samples from three well-studied impact craters were analyzed by optical microscopy, scanning electron microscopy (SEM), and Raman spectroscopy in thin section and grain separates. These samples are comprised of well-preserved, rapidly quenched impactites from the Ries crater, Germany, strongly annealed impactites from the Popigai crater, Siberia, and altered, variably quenched impactites from the Chicxulub crater, Mexico. The natural samples were compared with samples of experimentally shock-metamorphosed zircon. Below 20 GPa, zircon exhibits no distinct shock features. Above 20 GPa, optically resolvable planar microstructures occur together with the high-pressure polymorph reidite, which was only retained in the Ries samples. Decomposition of zircon to ZrO_2 only occurs in shock stage IV melt fragments that were rapidly quenched. This is not only a result of post-shock temperatures in excess of ~1700 °C but could also be shock pressure–induced, which is indicated by possible relics of a high-pressure polymorph of ZrO_2. However, ZrO_2 was found to revert to zircon with a granular texture during devitrification of impact melts. Other granular textures represent recrystallized amorphous $ZrSiO_4$ and reidite that reverted to zircon. This requires annealing temperatures >1100 °C. A systematic study of zircons from a continuous impactite sequence of the Chicxulub impact structure yields implications for the post-shock temperature history of suevite-like rocks until cooling below ~600 °C.

INTRODUCTION

Significance of Zircon as a Shock Indicator

Zircon is among the last minerals that succumb to shock deformation and the subsequent extreme temperature conditions (El Goresy 1965, 1968; Mashimo et al. 1983). It has been suggested that zircon preserves shock features even under granulite facies metamorphic conditions (Reimold et al. 2002). This allows the identification and dating of ancient impact structures, e.g., Sudbury (Krogh and Davis 1984; Krogh et al. 1996) and Vredefort (Kamo et al. 1996; Gibson et al. 1997; Reimold et al. 2002). A correlation of distal ejecta with parental impact structures was attained by the study of shocked zircons (Krogh et al. 1993a, 1993b). In spite of their importance, shock features in zircon are only occasionally described by in situ methods (El Goresy 1968; Kamo et al. 1996; Corfu et al. 2003). Grain separation from whole rocks will recover more zircons, but some shock features are commonly lost, e.g., decomposed zircon (Glass 2000; Deloule et al. 2001). Also, grain sizes below ~100 μm are seldom recovered (Krogh et al. 1993a, 1993b). This study aims to constrain the occurrence and stability of shock features in naturally shocked zircon from a known petrological context. In a case study from a continuous ejecta deposit from the Chicxulub crater, implications for the temperature-time history of this sequence will be discussed.

Previous Studies of Shock-Induced Features in Zircon

Reidite and Planar Microstructures

Naturally shocked zircons appear turbid to opaque in color (Krogh et al. 1984; Bohor et al. 1993; Corfu et al. 2003) and exhibit a decrease of the refractive index, which indicates amorphization (Dobretsov et al. 1969). Amorphous lamellae of diaplectic $ZrSiO_4$ glass were confirmed by transmission electron microscopy (TEM) analyses of experimentally shocked $ZrSiO_4$ (Leroux et al. 1999). They occur as multiple sets of intersecting planes with spacings between 0.5 and 4 μm that are optically not recordable. Optically recordable planar microstructures have been identified as microcracks and microtwinning features (Leroux et al. 1999; Reimold et al. 2002). They occur as single or multiple sets of parallel bands with a spacing below 5 μm (Krogh and Davis 1984;

Bohor et al. 1993) and are interpreted to form along with the transition of zircon to the high pressure polymorph reidite (Kusaba et al. 1986; Leroux et al. 1999; Finch and Hanchar 2003). The shock-induced martensitic, i.e., solid-state transition of zircon to reidite starts at ~20 GPa and is complete at 52 GPa (Fiske et al. 1994). Reidite is quenchable and stable at ambient pressures and temperatures up to 1000 °C. It fully reverts to zircon if heated at ambient pressures to 1200 °C (Kusaba et al. 1985). Reidite (space group $I4_1/a$) has a tetragonal structure akin to zircon (space group $I4_1/amd$) and exhibits similar optical properties but is about 10% more dense (Reid and Ringwood 1969; Kusaba et al. 1985; Leroux et al. 1999; Glass et al. 2002; van Westrenen et al. 2004). Natural reidite was found in distal ejecta from the Eocene Chesapeake Bay impact, where it occurs together with tektite glass, shocked quartz and feldspar, coesite and stishovite (Glass and Liu 2001; Glass et al. 2002). The only other occurrence was reported from a suevite melt fragment of the Ries crater (Gucsik et al. 2004a, 2004b).

Granular Textures

Granular-textured zircon grains are frequently observed in impact-related lithologies (Bohor et al. 1993; Krogh et al. 1993b, 1996; Glass and Liu 2001). Such polycrystalline grains represent crystallites of zircon in a glassy $ZrSiO_4$ matrix (Bohor et al. 1993; Kamo et al. 1996; Glass 2000) that resulted from shock-induced amorphization and subsequent recrystallization. Localized granular aggregates that were interpreted as incipient structural breakdown or recrystallization features were produced in shock experiments (Deutsch and Schärer 1990; Leroux et al. 1999).

Decomposition

The decomposition of zircon was first described by El Goresy (1965, 1968) in tektite glass and glassy melts of suevites as granular droplets of monoclinic ZrO_2 (baddeleyite) at rims of zircon clasts. This author inferred temperatures for this breakdown reaction between 1775 °C–1900 °C. The presence of this decomposition feature in tektites was consequently used to infer their origin from a hypervelocity impact (Kleinmann 1969; Glass et al. 1990, 1995). It is also regarded as a feature that is diagnostic of impact melts in general (Marvin and Kring 1992; Koeberl and Reimold 2003; Wittmann et al. 2004a, 2004b). Dobretsov et al. (1969) reported the decomposition of zircon to a mixture of ZrO_2 polymorphs, amorphous SiO_2, and amorphous $ZrSiO_4$ in shock experiments. This was confirmed by Kusaba et al. (1985) in shock recovery experiments at pressures of ~90 GPa.

SAMPLE DESCRIPTIONS

Ries Crater

The Ries crater in Germany, which is 14.4 Ma old and 24 km in diameter, is a well-preserved complex crater (e.g., Stöffler and Ostertag 1983; von Engelhardt 1990; Laurenzi et al. 2003). Impactites from the Ries have been studied in great detail and have revealed some basic principles of impact metamorphism (e.g., Hörz 1965; Stöffler 1971a, 1974a; von Engelhardt et al. 1969, 1995; von Engelhardt 1990, 1997; Newsom et al. 1990). Various ultra-high pressure minerals were found and intensely studied in Ries impactites, e.g., stishovite, coesite (Stöffler 1971b), diamond (e.g., Hough et al. 1995; El Goresy et al. 2001a; Schmitt et al. 2005), a post-diamond carbon polymorph (El Goresy et al. 2003), baddeleyite-structured TiO_2 (El Goresy et al. 2001b), and reidite (Gucsik et al. 2004a, 2004b).

We extracted highly shocked crystalline fragments from the fallout suevites of the Seelbronn, Zipplingen, and Aumühle locations in the Ries crater. Macroscopically, their high degrees of shock metamorphism are indicated by pumice-like textures. Microscopically, crystallized feldspar melt, diaplectic quartz glass with tube-like coesite, and thermally decomposed biotite are present in the Zipplingen and Seelbronn fragments. Following the shock classification of Stöffler (1971a), this suggests lower shock stage III conditions with equilibrium shock pressures of 45–50 GPa and post-shock temperatures of 900–1100 °C, given that feldspar melt is recrystallized but no ballen quartz crystallized and coesite is retained (Dworak 1969; Stöffler 1971b; Stöffler and Langenhorst 1994; Grieve et al. 1996). The only carbon phase observed in the Seelbronn fragment is impact diamond (Schmitt et al. 2005). Feldspar and quartz occur as diaplectic glasses in the fragment from Aumühle. This is diagnostic for shock stage II conditions of shock pressures between 35–45 GPa and post-shock temperatures <900 °C (Dworak 1969; Stöffler 1972; von Engelhardt 1990).

Two additional samples of the fallout suevites of Seelbronn and Aumühle represent inhomogeneous shock stage IV melt fragments that indicate peak shock pressures in excess of 60 GPa and post-shock temperatures >1500 °C (Stöffler 1971a; von Engelhardt 1990). The Aumühle sample is taken from a grey melt fragment with an aerodynamic, contorted shape. In thin section, the melt rock matrix appears almost completely crystallized with intergrown plagioclase phenocrysts and abundant cryptocrystalline Ti-Fe oxides. Pyroxene is missing as a liquidus phase in the melt matrix, indicating elevated f_{H2O} (von Engelhardt 1995). The shock stage IV sample from Seelbronn is a dark blue-grey melt fragment. In thin section, an agglutinated rim of lithic particles and a melt matrix devoid of phenocrysts can be observed. The core of this melt fragment exhibits abundant clinopyroxene phenocrysts as the only liquidus melt phase. This style of phenocryst crystallization is commonly interpreted as indicative of quenching under low f_{H2O} conditions or very rapid quenching from very high temperatures (von Engelhardt et al. 1995; Whitehead et al. 2002; Osinski 2003).

Popigai Crater

To characterize shock features in zircon from coherent impact melt rocks, we investigated two samples from the largest known Cenozoic impact structure, the Popigai crater in northern Siberia, which is 35.7 Ma old and 100 km in diameter (Masaitis 1994; Bottomley et al. 1997; Vishnevsky and Montanari 1999; Whitehead et al. 2002). The samples are from an outcrop in the crater (71°38′N, 11°12′E) and represent dark grey to black melt rock that incorporated various lithic clasts. Under the microscope, the samples exhibit hypo- and holocrystalline melt rock matrices with abundant hypersthene and labradorite phenocrysts and reaction coronas of hypersthene around quartz clasts. Monomineralic clasts occur, e.g., ballen quartz, quartz grains with several bands of decorated planar deformation features (PDFs), kink-banded, sometimes thermally decomposed biotite, checkerboard feldspar, and some without a distinct shock metamorphic overprint. Some polymineralic lithic clasts of shock stages I–III, e.g., gneiss fragments, were observed as well.

Chicxulub Crater

The Chicxulub impact structure on the Yucatán Peninsula, Mexico, has a diameter of ~180 km (e.g., Hildebrand et al. 1995; Morgan et al. 1997, 2000; Vermeesch and Morgan 2004) and was formed 65 million years ago (e.g., Hildebrand et al. 1991; Swisher et al. 1992). The ICDP-Yaxcopoil-1 borehole (Yax-1) was drilled about 62 km to the south-southwest of the center of the Chicxulub impact structure (Urrutia-Fucugauchi et al. 2004), within the annular trough between the peak ring and the crater rim. It encountered about 100 m of suevitic, impact melt rock-bearing breccias (Dressler et al. 2003, 2004; Stöffler et al. 2004; Tuchscherer et al. 2004a; Kring et al. 2004). These units are underlain by sedimentary "megablocks" (Kenkmann et al. 2004), in which Yax-1 terminated. The megablocks are predominantly composed of brecciated dolomite, limestone, anhydrite and some impact induced dike breccias (Wittmann et al. 2004b). Because of the scarcity of clastic sedimentation in the sedimentary target sequence (López Ramos 1975), zircon was almost exclusively derived from crystalline target rocks of pan-African age (Krogh et al. 1993b). We analyzed 17 thin sections of samples from Yax-1 that comprise suevites, impact melt rocks, and dike breccias (Fig. 1).

Experimentally Shocked Samples

Thin sections of non-metamict zircon that was experimentally shocked to 38, 40, 60 and 80 GPa at the Ernst Mach Institute in Germany were available for analysis. These samples were previously described by Leroux et al. (1999), Reimold et al. (2002), and Gucsik et al. (2004a, 2004b) (Figs. 2a and 2b).

ANALYTICAL METHODS AND REFERENCE MATERIALS

The zircon grains were found by systematic scanning of 24 thin sections in high-contrast backscattered electron mode (BSE) under the scanning electron microscope. Some $ZrSiO_4$ grains were checked for their major element composition by energy dispersive spectroscopy (EDX) before wavelength dispersive (WDX) compositional mapping under the electron microprobe was performed to confirm the presence of ZrO_2 next to $ZrSiO_4$. To collect qualitative structural information, microRaman spectroscopy was performed on a notch filter based Dilor LabRam spectrometer, with a He-Ne laser of 632.8 nm wavelength. The energy of 3 mW was transferred to the sample with a spot size of ~1 μm. Spectra were recorded by three-fold accumulation and collection times between 3 and 100 seconds, with a thermoelectrically cooled CCD detector operated with a 1800 grooves/mm grating in the frequency range between 200–1200 cm^{-1}. The wave number accuracy is about 1 cm^{-1}. Background reduction was achieved by Gauss-Lorenz fitting using the LabSpec v.2.08 software by Dilor SA and Université de Reims. Details on the deconvoluting procedure are given in Nasdala et al. (2001) and references therein. Additionally, we investigated three grain separates of shock stage III gneiss samples from Seelbronn and Zipplingen and the shock stage IV impact melt samples from Aumühle by optical microscopy and microRaman spectroscopy. The $ZrSiO_4$ grains are a residue from cyclic acid dissolution by application of HF, HCl, and H_3BO_3 as described in Schmitt et al. (2005). Four of these $ZrSiO_4$ grains from the Zipplingen sample were subsequently mounted on a thin section for SEM analysis. As reference materials for Raman spectroscopy, a thin section of natural zircon from Australia and baddeleyite from the Phalborwa carbonatite taken from the collections of the Museum für Naturkunde were used.

RESULTS

Experimentally Shocked $ZrSiO_4$

All measurements of the experimentally shocked zircon (Fig. 3) agree with previously published Raman spectra of reidite (Gucsik et al. 2004a, 2004b). Reidite is the only phase in the samples shocked to 40, 60, and 80 GPa and background intensities increase until 60 GPa before they decrease toward the level of the unshocked precursor in the 80 GPa sample (Fig. 3). We did not find relics of zircon coexisting with reidite in the sample shocked to 40 GPa, which have been described by other authors (Leroux et al. 1999; Gucsik et al. 2004a, 2004b). Scarce relics of zircon coexisting with reidite were found in the sample shocked to 38 GPa with very low intensities and broad half-widths (FWHM) of 10.6 and 13.4 cm^{-1} from initial average values of 2–4 cm^{-1} in the unshocked material, which indicates shock-induced

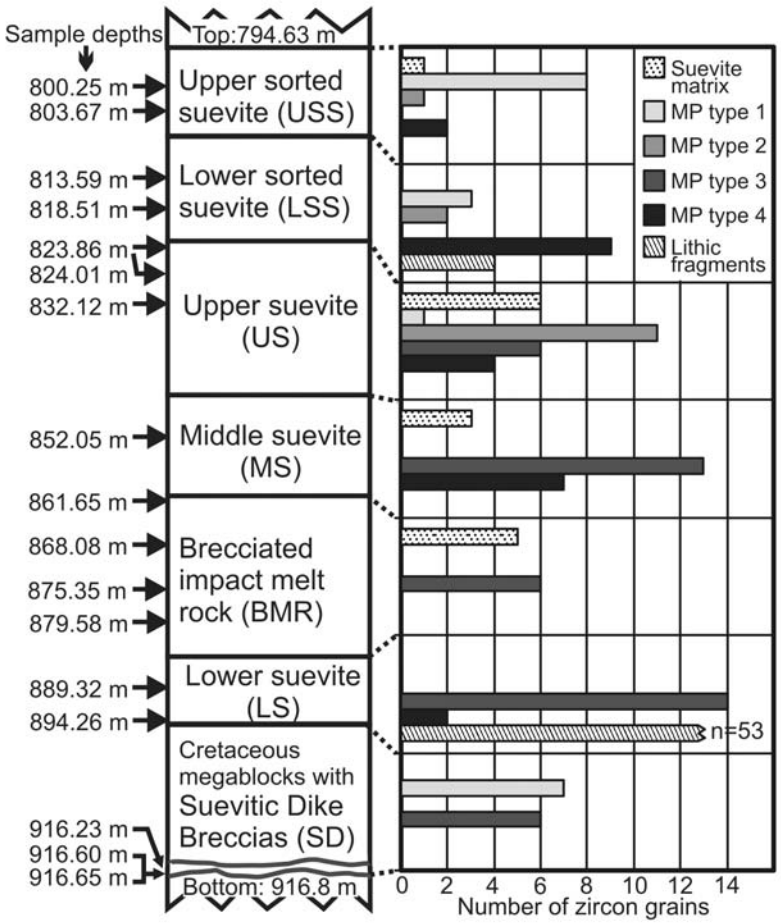

Fig. 1. A schematic profile of the analyzed section of Chicxulub drill core Yaxcopoil-1 and host materials of zircons as encountered in the respective units. Sample locations are indicated with their respective depths; unit nomenclature after Stöffler et al. (2004). Melt particles (MP) type 1 exhibit brownish green colors, amoeboid shapes, and frequently perlitic textures and are commonly lacking phenocrysts (Hecht et al. 2004; Tuchscherer et al. 2004b). MP type 2 contain abundant vesicles, have green to brown colors, and have crystallized some feldspar phenocrysts. Some exhibit shard morphologies with armored rims of accreted fine particles from the ejecta plume. MP type 3 have mostly white to brownish colors and generally exhibit abundant plagioclase and diopside phenocrysts in an altered melt matrix. MP type 4 are dark brown and contain finely disseminated iron oxides and variably abundant feldspar phenocrysts. The suevite matrix is composed of mineral fragments and melt particles and suffered variable degrees of hydrothermal overprint by calcite and hematite (Stöffler et al. 2004). Kring et al. (2004) and Dressler et al. (2004) discuss the possibility that the matrix had been in a melted state shortly after emplacement. The lithic fragment in a lower sorted suevite (LSS) sample is an amphibolite facies calc-silicate. Quartz and plagioclase exhibit decorated PDFs and biotite displays kink bands, indicating lower shock stage I conditions of shock pressures between 10 and 20 GPa (Stöffler 1971a; Stöffler and Langenhorst 1994; Grieve et al. 1996). The lithic fragment from the lower suevite (LS) sample is a dm-size granite. The granitic fabric is retained, although the mineral components suffered intense thermal overprint. Biotite is thermally decomposed, feldspar is mostly recrystallized and PDFs in quartz are decorated. This indicates upper shock stage I conditions of 20 to 35 GPa.

amorphization (Gucsik et al. 2004b). In contrast to other studies, we did not find indications of granularization or decomposition in the samples shocked to 60 and 80 GPa (Kusaba et al. 1985; Deutsch and Schärer 1990; Leroux et al. 1999).

Ries Crater

Lithic Fragments of Shock Stage II–III

The three thin sections of the Zipplingen and Seelbronn samples yielded $ZrSiO_4$ grains (Fig. 4; Table 1), which show intense undulous extinction under the optical microscope. Most grains are associated with recrystallized shock melts of plagioclase and biotite. Other host materials are cordierite, diaplectic quartz glass with coesite inclusions (Figs. 5a and 5b), sillimanite, titanite, and kink-banded biotite. Maskelynite as a host is only retained in the shock stage II sample from Aumühle.

All grains analyzed in the sample from Zipplingen, including those in the grain separate, indicate the presence of reidite together with zircon. Some $ZrSiO_4$ grains in the Seelbronn and Aumühle samples indicate the sole presence of

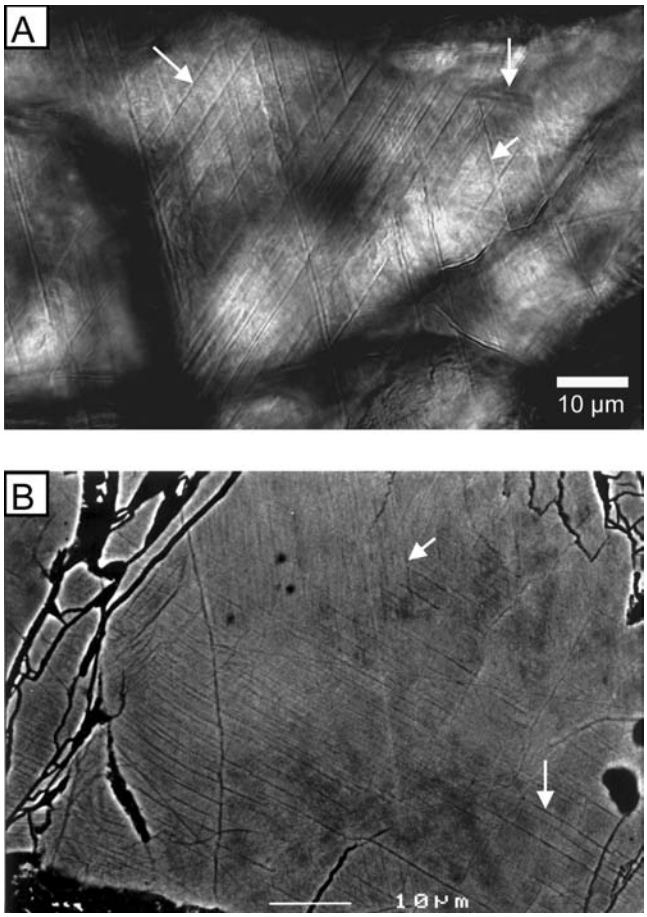

Fig. 2. $ZrSiO_4$ experimentally shocked to 60 GPa that transformed to reidite. a) Plane-polarized light micrograph displays three bands of planar microstructures, as indicated by arrows. b) Scanning electron microscope (SEM), backscattered electron mode (BSE) image indicates two bands of planar microstructures.

zircon. Reidite-zircon grains exhibit zoning patterns in discrete domains and sub-parallel lamellae of sub-µm thicknesses and spacings (Figs. 5b and 5c). Raman spectra show variable intensity ratios of the indicative v_3 Raman bands of zircon that span a range of frequencies and full widths at half maximum (FWHM) (Figs. 5d and 6) that are in accordance with the amorphization trends of relic zircon domains in experimentally shocked $ZrSiO_4$ (Gucsik et al. 2004b). Raman mapping of relic compositional zoning areas reveal the predominance of zircon in areas with a high degree of impurities, while reidite-zircon occurs in unzoned regions (Figs. 7a and 7c). A granular texture occurs only at an incipient stage at the rim of one grain (Fig. 5c) from the Zipplingen sample. Reidite was not found in this granular textured rim (Fig. 5d). No ZrO_2 was indicated in SEM-EDX analyses and backscattered images or microRaman spectroscopic analyses.

Reflected light microscopy was applied to analyze the grain separate samples with regard to shock features. These observations were checked by SEM imaging of thin sections

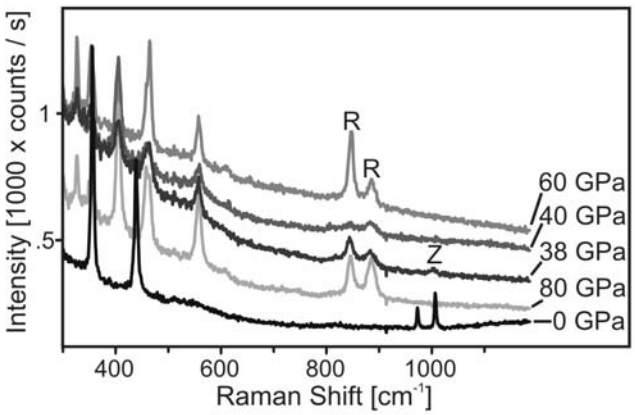

Fig. 3. Raman spectra of experimentally shocked $ZrSiO_4$ specimen and unshocked zircon that were taken at identical measurement conditions. Indicative zircon band positions (Z) and those of reidite (R) are only coexisting in the sample shocked at 38 GPa.

of four of these grains. These SEM images revealed large voids and granular textures together with domains of smooth surfaces with planar microstructures (Fig. 7d). MicroRaman spectroscopy confirmed the presence of reidite in the grain separate samples (Table 1) and therefore verified the thin section analyses. Moreover, this is evidence for the resistance of reidite to acid treatment. However, the presence of granular textures and voids (Fig. 7d) indicates the dissolution of one component of the $ZrSiO_4$ grains, most likely an amorphous phase.

Lithic Fragments of Shock Stage IV

A large percentage of $ZrSiO_4$ grains in the two thin sections from Aumühle and Seelbronn (Fig. 4; Table 1) exhibit undulous extinction under the microscope. All grains are embedded in the melt matrices. Most of the granular textured zircon grains appear very porous with dark brown to black colors and are barely birefringent. However, about half of the granular textured grains from the more strongly devitrified sample from the Aumühle sample are polycrystalline with regular optical properties.

The fraction of grains that exhibit coronas of ZrO_2 granules (Figs. 8a and 8b) are mostly associated with granular textured zircon, but intergrowths with fractured single grain zircon occur as well and one grain is completely decomposed to ZrO_2 (Fig. 8c). All grains analyzed with decomposition coronas yield Raman spectra of baddeleyite (López et al. 2001). This is indicated by the most prominent and distinct Raman band of baddeleyite at ~474 cm^{-1} (Fig. 9). The indicative band of the tetragonal ZrO_2 polymorph at ~270 cm^{-1} (López et al. 2001) was not found. Because the cubic high temperature polymorph of ZrO_2 is reported to only display one Raman band at 616 cm^{-1} that also occurs in the Raman spectrum of baddeleyite (López et al. 2001), this polymorph coexisting with baddeleyite can not be verified by Raman spectroscopy. Four of the grains

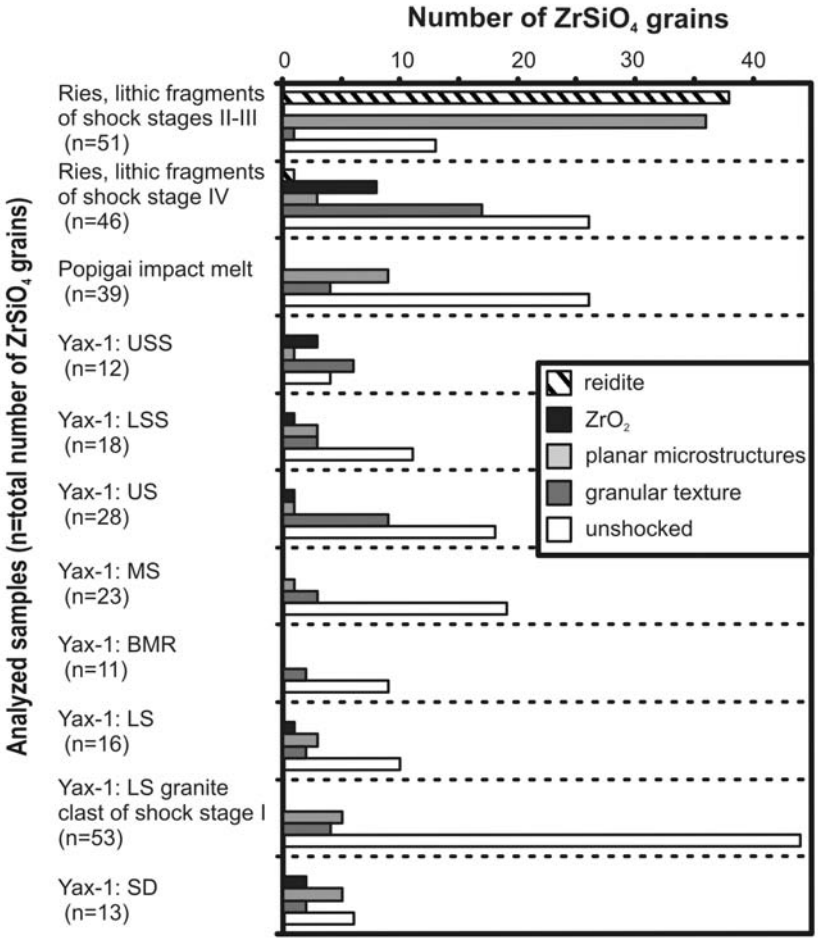

Fig. 4. Absolute abundance of shock-induced features in the $ZrSiO_4$ grains analyzed in thin section. Single grains may exhibit multiple shock features, e.g., reidite and planar microstructures or granular textures and ZrO_2; therefore, abundances of shock features plus unshocked grains do not generally add up to the sum of analyzed grains. Abbreviations as introduced in Fig. 1.

Table 1. Statistical data for natural $ZrSiO_4$ grains. Thin section analyses unless noted otherwise.

Sample types	Number of grains	Min.–max. size (μm)	Median size (μm)	Planar micro-structures (%)	Granular textures (%)	Decomposed to ZrO_2 (%)	Reidite (%)	Total shock features (%)
Ries, lithic fragments of shock stages II–III	51	15–191	54	71	2	n.d.	75	75
Ries, lithic fragments of shock stages II–III, grain separates	16	45–341	121	19	25	n.d.	88	94
Ries, clasts in shock stage IV	46	18–90	44	7	37	17	2	43
Ries, clast in shock stage IV, grain separate	11	67–179	105	36	27	n.d.	n.d.	55
Popigai impact melt	39	19–131	43	23	10	n.d.	n.d.	33
Yax-1: USS[a]	12	8–115	25.5	8	50	25	n.d.	67
Yax-1: LSS[a]	18	8–52	20	17	17	6	n.d.	39
Yax-1: US[a]	28	10–102	20.5	4	32	4	n.d.	36
Yax-1: MS[a]	23	13–67	17	4	13	n.d.	n.d.	17
Yax-1: BMR[a]	11	12–70	20	n.d.	18	n.d.	n.d.	18
Yax-1: LS[a]	16	13–86	22	19	13	6	n.d.	38
Yax-1: LS[a] granite clast of shock stage I	53	15–110	39.5	9	8	n.d.	n.d.	17
Yax-1: SD[a]	13	14–183	36	38	15	15	n.d.	54
Yax-1 total	174	8–183	27	11	17	5	n.d.	30

[a]Unit abbreviations as introduced in Fig. 1.

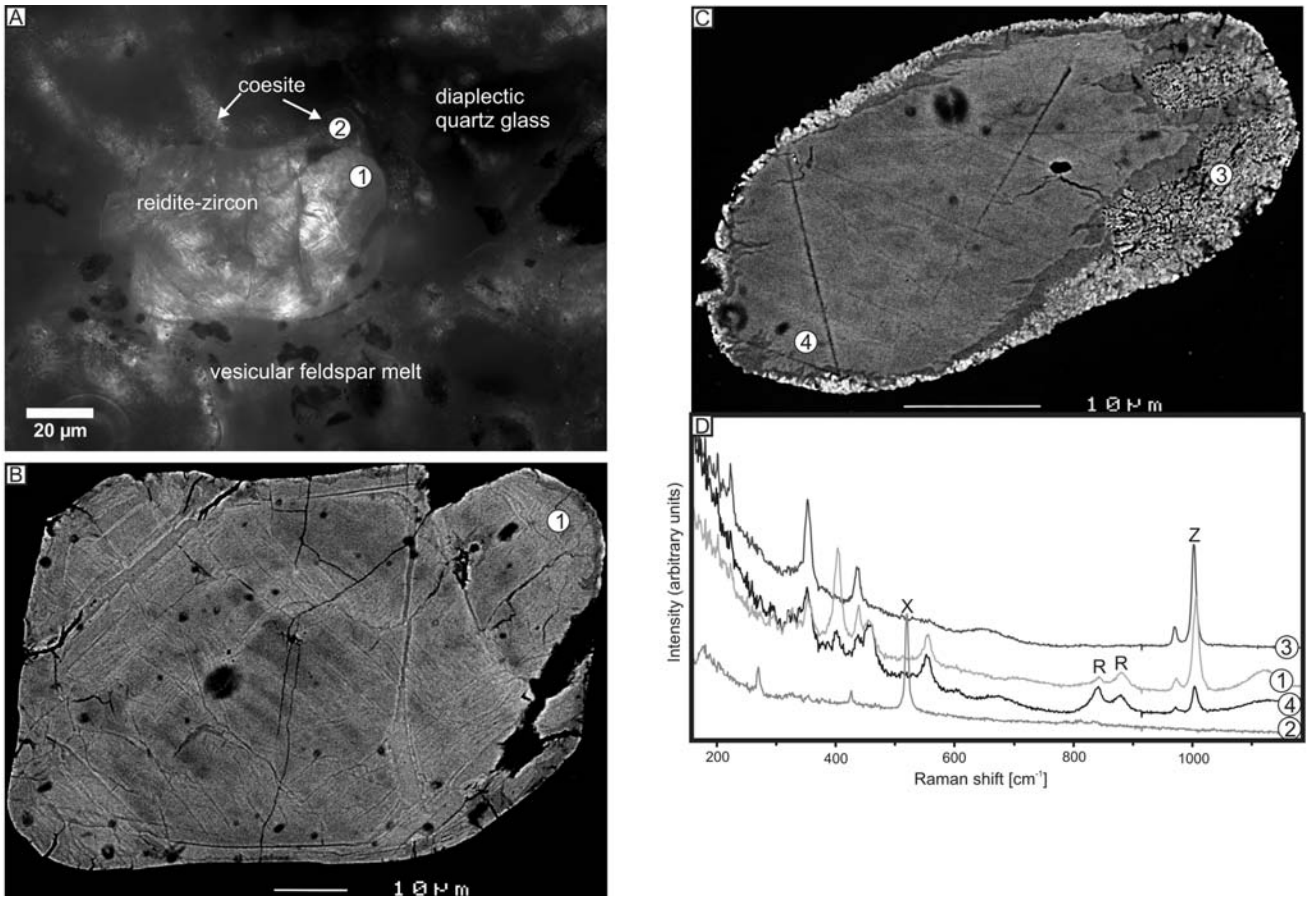

Fig. 5. Reidite from the Ries crater. a) and b) Reidite-zircon grain with complex zoning pattern and planar microstructures associated with coesite, diaplectic quartz glass, and vesicular feldspar melt in the shock stage III sample from Zipplingen (optical microscope, crossed polarizers and SEM-BSE image, respectively). c) Reidite-zircon grain associated with vesicular, recrystallized plagioclase melt in shock stage III sample from Zipplingen. Note the rim with a granular texture (SEM-BSE image). d) Raman spectra of domains indicated with labels in (a), (b), and (c): (1) reidite-zircon, respective band frequencies for reidite (R) are –842 cm^{-1} and 880 cm^{-1} and for zircon (Z) –1006 cm^{-1}; (2) coesite with the indicative peak frequency at 518 cm^{-1} (X); (3) zircon (Z) spectrum of the granular rim with frequency of 1001 cm^{-1}; and (4) reidite-zircon spectrum of core with frequency of (Z) at 1003 cm^{-1} and (R) at 839 cm^{-1} and 878 cm^{-1}.

with decomposition coronas yield spectra with the indicative band of the orthorhombic-II ZrO_2 polymorph at 661 cm^{-1} (Arashi et al. 1990; Haines et al. 1997) (Fig. 9).

One grain in the more rapidly quenched sample from Seelbronn exhibits a high density of planar microstructures and Raman spectra of coexisting reidite and zircon. Otherwise, planar microstructures occur as parallel bands of tiny bubbles in zircon with spacings below 1 µm. Interestingly, the grain separate sample from Aumühle displays the exclusive presence of zircon while decomposed grains are missing altogether and planar microstructures seem to be accentuated (Table 1).

Popigai Crater

Two-thirds of the $ZrSiO_4$ grains in the two thin sections are embedded in the melt matrix and one-third are associated with lithic clasts that float in the melt matrix. $ZrSiO_4$ grains that are inclusions in kink-banded biotite, quartz with decorated PDFs, and quartz without shock features do not show impact-induced features. All $ZrSiO_4$ grains that are intergrown with ballen quartz or polycrystalline feldspar (Figs. 10a and 10b) exhibit shock features. Two granular textured $ZrSiO_4$ grains with dark brown colors occur in the melt matrix. One of these grains indicates incipient isotropization (Figs. 10c and 10d), while the other one displays regular optical properties of a polycrystalline texture. Another two granular-textured grains are inclusions in a cm-size gneiss fragment with annealed features of shock stage III. These $ZrSiO_4$ grains have brown colors (Figs. 10e and 10f) and appear partially recrystallized. Decorated planar microstructures with spacings of 1–4 µm and widths << 1 µm (Figs. 10a and 10b) occur in translucent to light brown grains that show dense fracture patterns. All $ZrSiO_4$ grains display Raman spectra of zircon without indications of advanced metamictization (Fig. 11), reidite or ZrO_2 (Table 1). The

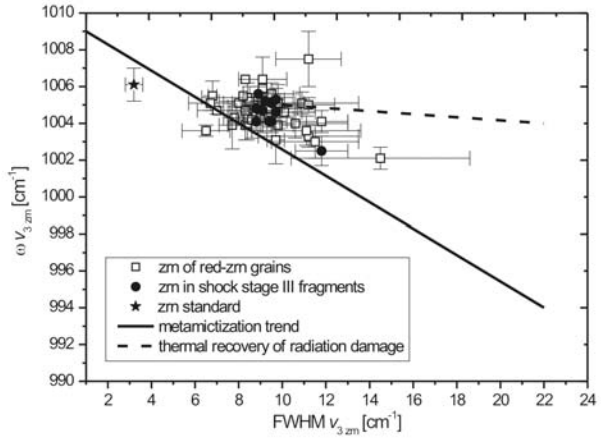

Fig. 6. Full width at half-maximum (FWHM) plotted versus frequency of Raman shift (ω) of the ν_3 anti-symmetric stretching mode of Si-O in zircon in the Raman spectrum of reidite-zircon and zircon grains from shock stages II–III and IV samples from the Ries crater, respectively. Error bars indicate standard deviation of a mean from multiple spectra of the same grain. For reference, means and standard deviation of 15 measurements of natural, unshocked zircon is plotted. The solid line indicates the trend of natural radiation damage of zircon after Nasdala et al. (2002) and Geisler and Pidgeon (2002). Trend of thermal recovery of radiation damaged zircon after Geisler and Pidgeon (2002).

variations in zircon ν_3 band FWHM and frequencies is smaller in comparison to the grains analyzed in the Ries and Chicxulub samples, indicating less amorphous zircon and therefore more pronounced thermal annealing.

Chicxulub Crater

The 17 thin sections from drill core Yax-1 yielded $ZrSiO_4$ grains that are mostly associated with melt particles. About one third of them occur in shock stage I crystalline rock fragments. Figure 1 displays the relative distribution of $ZrSiO_4$ host particles in the units of Yax-1 and Fig. 12 shows the proportions of shocked $ZrSiO_4$ grains in these hosts.

Grains that bear planar microstructures exhibit regular to reduced birefringence and clear to light brown colors. One fourth of them display two to three bands of sub-µm wide planar features that intersect at various angles (Figs. 13a and 13b). The rest show bands of pores in one to two directions that are reminiscent of "decorated" PDFs (Figs. 13c and 13e).

$ZrSiO_4$ grains with granular textures were found in every unit from the analyzed section of Yax-1 (Fig. 1; Table 1). Two-thirds of these grains are of a dark brown color and exhibit strongly reduced birefringence and a high density of nm-size vesicles (Fig. 14a). One-third appears more strongly recrystallized to a polycrystalline texture (Figs. 14b and 14e). Only a fraction of the grains in one of the shock stage I crystalline basement fragments analyzed exhibit shock features (Table 1). These grains belong to the granite fragment that experienced upper shock stage I pressures >20 GPa.

Generally, two styles of decomposed $ZrSiO_4$ grains can be distinguished. First, the "quenched" type, which displays coronas of separate ZrO_2 granules around a zircon core (Figs. 15a–d). This type is like the decomposed grains from the Ries samples (Figs. 8a–c). It occurs in two-thirds of the decomposed grains and all of them are associated with type 1 melt particles in the uppermost units of Yax-1. The other type occurs as vermicular intergrowths of ZrO_2 with zircon near the rim in grains that are associated with type 1 and type 3 melt particles (Figs. 15e–g). This suggests incipient breakdown (Figs. 15e and 15f) and recovery (Fig. 15g), respectively. ZrO_2 associated with granular textured zircon (Figs. 15a–d) was confirmed by Raman spectroscopy in about 13% of the granular textured zircon grains. However, SEM images and EDX-qualitative analyses indicate that ZrO_2 may be present in far more granular textured grains as nm-size round entities with a high mass contrast.

Featureless $ZrSiO_4$ grains in Yax-1 yield Raman spectra that range from those of well-crystallized zircon with Raman shifts of the ν_3 band of ~1005–1008 cm^{-1} and FWHM of 3–5 cm^{-1} to rare examples of moderately disordered crystalline structures with frequencies <1000 cm^{-1} and FWHM of ~20 cm^{-1} (Nasdala et al. 2004) (Fig. 16). No spectra of reidite or strongly metamict zircon were recorded. Raman spectra of zircon grains with planar microstructures are not distinguishable from those of the "unshocked" specimens (Fig. 16). Granular textured grains exhibit Raman characteristics that overall follow the trend of natural irradiation damage of Nasdala et al. (2002) and Geisler and Pidgeon (2002). Plots of FWHM versus Raman shift for the zircon components of ZrO_2-zircon intergrowths indicate large variations and a wide spread of frequencies compared to the other zircon spectra (Fig. 16). This suggests higher degrees of amorphization compared to all other shocked zircons analyzed. All Raman spectra of ZrO_2 coexisting with zircon indicate the presence of baddeleyite (López et al. 2001). Two grains (one example in Figs. 15a and 15b) in the uppermost suevite units upper sorted suevite (USS) and lower sorted suevite (LSS) display Raman spectra with bands at 661 cm^{-1} that may indicate the presence of relics of the orthorhombic II polymorph of ZrO_2.

DISCUSSION

Planar Microstructures and Reidite

Planar microstructures in zircon develop along with the transition to reidite (Leroux et al. 1999; Reimold et al. 2002; Finch and Hanchar 2003). This transition occurs in a mixed phase regime of pure zircon and reidite between 20–52 GPa (Fiske et al. 1994) (Fig. 17) and results in an ~10% decrease in volume (Reid and Ringwood 1969; Kusaba et al. 1985;

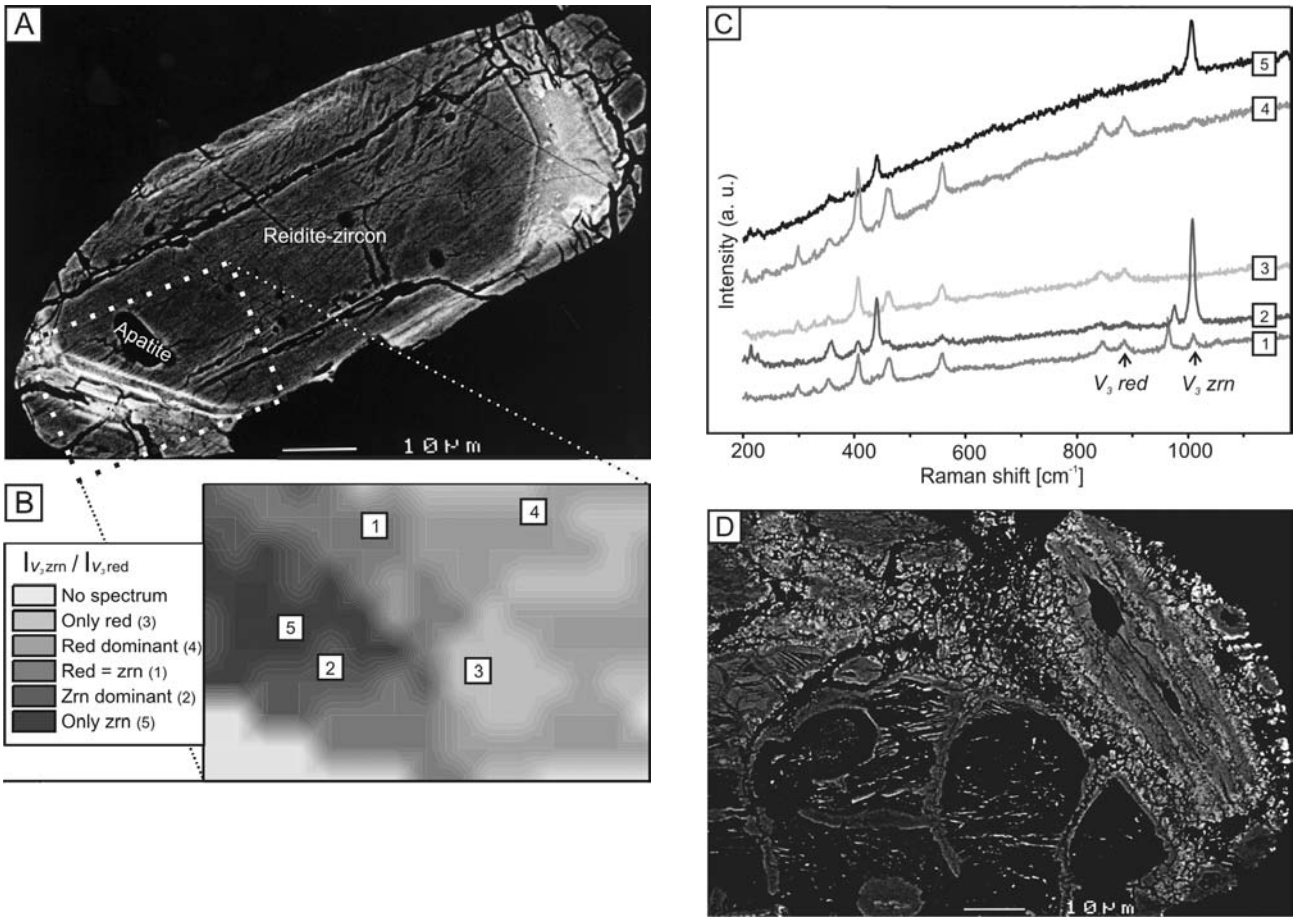

Fig. 7. a) Compositionally zoned zircon-reidite grain embedded in recrystallized, vesicular plagioclase melt of shock stage III sample from Seelbronn, Ries crater (SEM-BSE image). b) Raman mapping of reidite-zircon area indicated in (a). Ratio of the ν_3 bands of zircon (zrn) and reidite (red) at ~1006 cm^{-1} and ~880 cm^{-1}, respectively. c) Single Raman spectra of exemplary measurement spots (1–5) in (b). Note the presence of the indicative band of apatite at 962 cm^{-1} in spectrum (1). d) Zircon-reidite grain from acid treated grain separate of the shock stage III fragment from Zipplingen (thin section SEM-BSE image).

Knittle and Williams 1993). Analyses of the experimentally shocked $ZrSiO_4$ samples reveal that the 60 and 80 GPa samples exhibit the most pronounced development of optically recordable planar microstructures (Figs. 2a and 2b). Conspicuous "trails of bubbles" that frequently occur in zircon grains with regular optical properties from the samples of Yax-1 and Popigai likely represent "decorated" PDFs (Grieve et al. 1996; Kamo et al. 1996; Leroux and Doukhan 1996; Moser 1997) that were formed due to a thermally induced crystallization of diaplectic $ZrSiO_4$ glass in these features. Paragenetic relations of these decorated PDFs from the Popigai and Yax-1 samples suggest post-shock thermal annealing in shock stage IV materials at temperatures of ~1200 °C (*T-t* paths [d–g] in Fig. 18). Because no decorated PDFs occur in the reidite-zircon grains from the Ries samples, 1200 °C is the best approximation for an upper limit for post-shock temperatures regarding the preservation of pristine PDF in zircon. The preservation of PDFs and reidite may thus be restricted to shock stages I-III of non-porous quartzo-feldspathic rocks. Exceptions can occur in components of shock stage IV impact melts that experienced very rapid quenching as evidenced by the sample from Seelbronn (Ries crater) (*T-t* path [c] in Fig. 18). We found that reidite occurs almost always in shock stages II–III fragments of the Aumühle, Seelbronn, and Zipplingen suevite deposits of the Ries crater. This petrologic context indicates formation conditions under equilibrium shock pressures of 35–50 GPa and post-shock temperatures of 300–1200 °C followed by rapid quenching (*T-t* path [a] in Fig. 18). No back-transformation of reidite to zircon due to grain separation processes, acid leaching, and Raman or SEM analysis were noticeable in our analyses of zircon-reidite from the Ries crater.

The occurrence of reidite intergrown with zircon in naturally shocked $ZrSiO_4$ is unlike the experimentally shocked zircons that indicate near complete conversion to the high-pressure polymorph at comparable shock pressure ranges. Because shock experiments represent a simplification

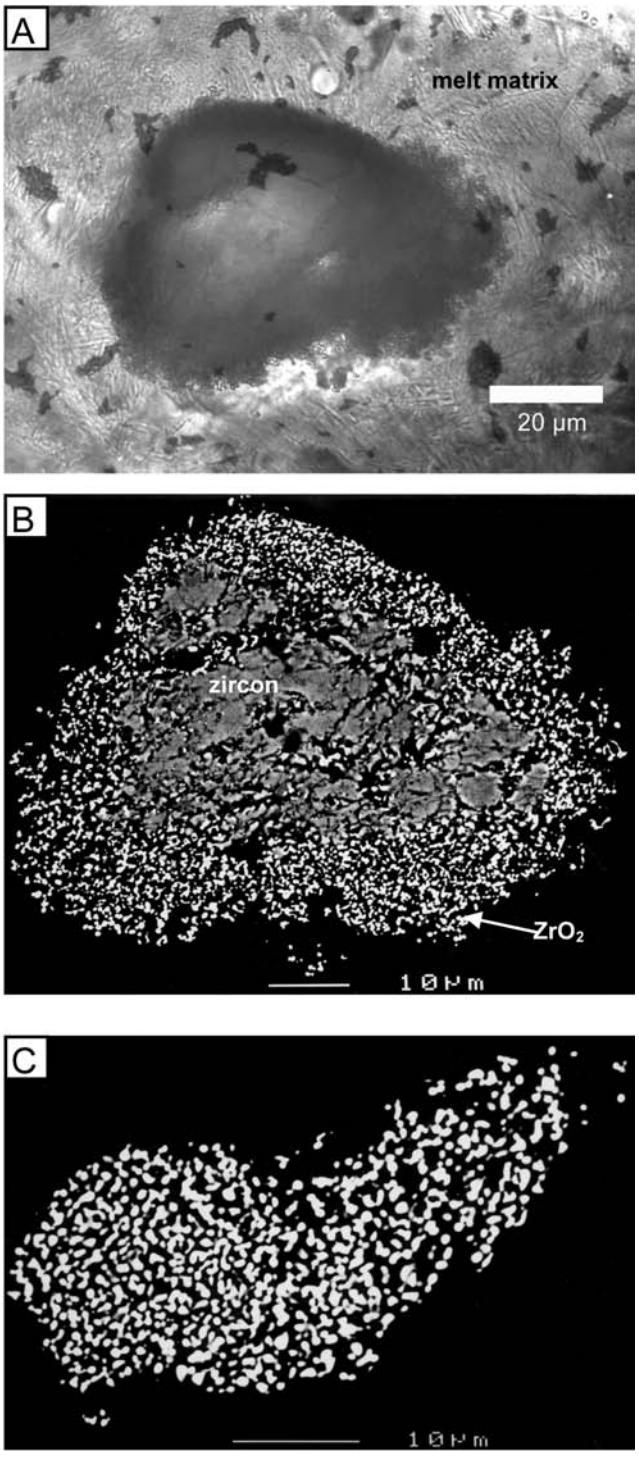

Fig. 8. a) and b) Partly decomposed, black zircon grain in glassy matrix with pyroxene phenocrysts of shock stage IV sample from Seelbronn, Ries crater. Optical microscope, plane-polarized light and SEM-BSE image, respectively. A core of granular textured zircon is retained while the rim region exhibits µm-size granules of ZrO_2. c) Decomposed zircon grain in shock stage IV sample from Seelbronn. The ZrO_2 granules are enclosed in the glassy melt matrix (SEM-BSE image).

of natural shock events, certain limitations apply, most notably in the duration of the shock wave (e.g., Stöffler 1972; Grieve et al. 1996) and the development of post-shock temperatures. These may be significantly lower in shock experiments than in naturally shocked samples (DeCarli et al. 2002). Gucsik et al. (2004a, 2004b) interpreted the difference between natural occurrence of reidite-zircon and experimental evidence as being due to heterogeneous shock pressures in natural impactites. Therefore, these authors suggested lower shock pressures for their zircon-reidite sample than indicated by petrography. However, heterogeneities in shock are commonly induced by positive pressure and temperature excursions from the equilibrium shock conditions (Stöffler and Langenhorst 1994; Heider and Kenkmann 2003). For example, micrometer-size hotspots that can occur during the shock compression of porous solids (DeCarli et al. 2002) must be considered for zircon, which is prone to developing porosities from auto-irradiation. This could explain a temperature-induced partial back-transformation of reidite to the zircon structure at equilibrium post-shock temperature conditions that are insufficient to crystallize diaplectic quartz glass, which occurs at temperatures of ~1100 °C (Rehfeldt-Oskierski et al. 1986; Grieve et al. 1996). Another explanation for the inhomogeneous occurrence of reidite in shock stage III samples could be impurities (Figs. 7a–c), which were shown to hamper the transformation to reidite (van Westrenen et al. 2004). Additionally, pre-existing metamictization may inhibit the transformation to reidite during a shock event because the martensitic transformation process, as proposed by Kusaba et al. (1986), requires a pre-existing zircon lattice. A certain degree of metamictization may result in the failure to contain the shear strain during distortion of the lattice relics and consequently result in shock-induced amorphization. The physical expression of this process may lie in the substantial decrease of the elastic moduli of zircon with increasing radiation damage (van Westrenen et al. 2004, and references therein).

Decomposition of Zircon

At ambient pressures, pure zircon decomposes at 1676 °C to a mixture of cristobalite and tetragonal ZrO_2 (Butterman and Foster 1967). ZrO_2 is known to occur in six different polymorphs of which only baddeleyite, the monoclinic low-temperature and low-pressure polymorph, and the orthorhombic II high-pressure polymorph are stable at ambient conditions (Arashi et al. 1990). All other polymorphs (tetragonal, cubic, hexagonal, and orthorhombic I) result from displacive transformations and consequently revert to baddeleyite at ambient pressure and temperature (Ohtaka et al. 1994; Haines et al. 1997). Because baddeleyite cannot be the primarily resultant polymorph of temperature and/or

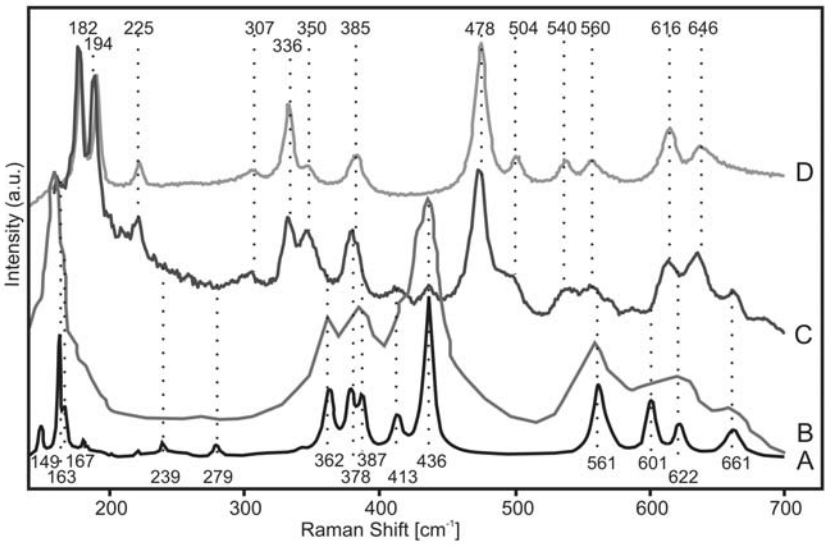

Fig. 9. Raman spectra of ZrO_2. Line A is a high-resolution orthorhombic II ZrO_2 spectrum that is redrawn after Haines et al. (1997); line B is a low-resolution orthorhombic II ZrO_2 spectrum, redrawn after Arashi et al. (1990); line C is from a partly decomposed grain of the shock stage IV sample from Aumühle, Ries crater, that indicates the presence of baddeleyite, zircon, and possibly orthorhombic II ZrO_2; and line D is from natural monoclinic ZrO_2 (baddeleyite) from Phalborwa. Note that the most prominent band of orthorhombic II ZrO_2 at 436 cm^{-1} also occurs in zircon. Dotted lines are visual guides; peak indication after López et al. (2001) on top refers to baddeleyite, on bottom after Haines et al. (1997) to orthorhombic II ZrO_2.

pressure induced decomposition of $ZrSiO_4$ (Butterman and Foster 1967; Ohtaka et al. 1994), relics of other polymorphs are to be expected in decomposed $ZrSiO_4$. In the decomposed $ZrSiO_4$ from the Ries and Chicxulub craters, we found zircon, baddeleyite and possible relics of the orthorhombic II polymorph of ZrO_2. This polymorph is stable above 1000 °C and >70 GPa and quenchable (Haines et al. 1997). We could not detect all the characteristic Raman bands of this polymorph. This problem was previously attributed to low spectral resolution and residual strain (Haines et al. 1997). Orthorhombic II ZrO_2 was shown to form in shock experiments at pressures above 80–90 GPa (Mashimo et al. 1983; Kusaba et al. 1985). Such possible relics of a pressure-induced decomposition were only detected in grains that are associated with rapidly quenched impact melt particles (Figs. 8a, 8b, 15a, and 15b). In contrast, grains that indicate reversion to zircon are mostly associated with melt particles that bear liquidus phase phenocrysts in Yax-1 (Figs. 15e–g).

Granular Textured Zircon

The onset of formation of granular textures in $ZrSiO_4$ was found in the Ries shock stage III samples. Although the grains barely exhibit granularization in thin section, the occurrence of grains with domains of reduced optical properties was revealed as shock induced amorphization in the grain separates of the same samples. The amorphous $ZrSiO_4$ was dissolved during acid treatment (Fig. 7d), confirming previous findings of granular textures in zircon-reidite intergrowths in the distal ejecta of the Chesapeake Bay impact after etching with acids and alkalies (Glass and Liu 2002).

Further formation conditions of granular textured $ZrSiO_4$ can be deduced from the occurrence as inclusions in ballen quartz (Figs. 10e and 10f). Ballen quartz is characteristic for the devitrification of diaplectic quartz glass, which was shown to occur at temperatures >1100–1300 °C in annealing experiments (e.g., Short 1970; Stöffler 1974b; Rehfeldt-Oskierski et al. 1986; Stöffler and Langenhorst 1994; Grieve et al. 1996). $ZrSiO_4$ that occurs in diaplectic quartz glass does not exhibit granular textures but consists of zircon and reidite intergrowths (Figs. 5a, 5b, and 5d). This suggests that some granular textures form due to the reversion of reidite to zircon, which results in a lattice expansion by ~11%.

We found that a recovery of optical properties accompanies a continuum of granular textures that ranges from grains with a high density of "microvesicles," suggestive of degassing in a $ZrSiO_4$ melt (Figs. 10d and 14a), to grains that recrystallized to μm-size euhedral crystallites (Figs. 14b–e). Raman spectroscopy indicates variations in crystallinity of the granular textured zircon grains that do not substantially differ from the "unshocked" grains (Figs. 11 and 16). Accounts of Raman spectra of "zircon glass" are scant and ambiguous in the literature. It can tentatively be assumed that diaplectic zircon glass should yield Raman spectra that resemble those of strongly metamict zircon (e.g., Nasdala et al. 2001, 2002, 2004; Geisler and Pidgeon 2002; Zhang et al. 2000a, 2004b). However, such spectra were not obtained in any measurements of this study. Also, additional Raman bands, as indicated by Gucsik et al. (2004b) from

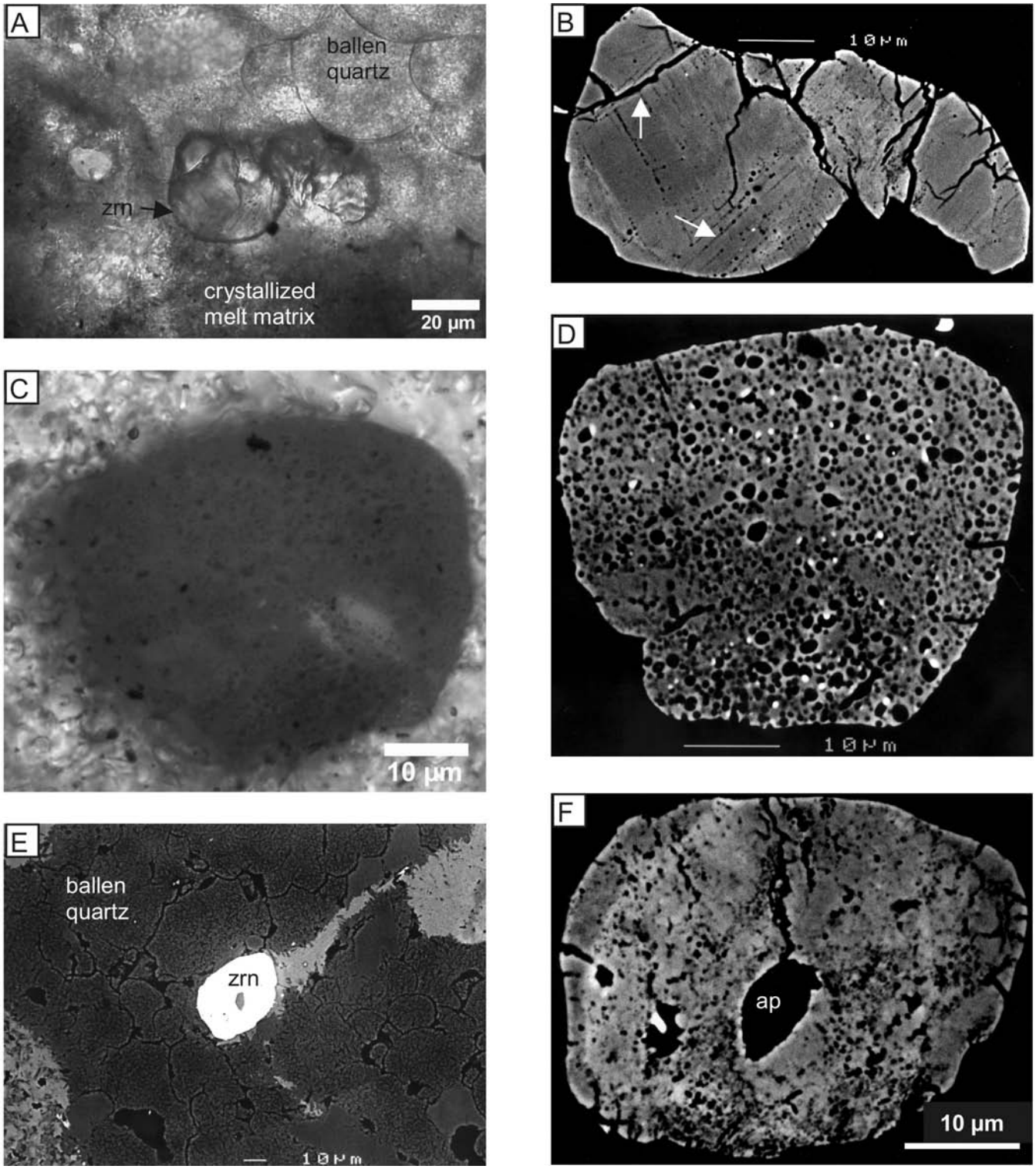

Fig. 10. Popigai impact melt rock samples. a) and b) A zircon grain with two sets of intersecting planar microstructures that is intergrown with ballen quartz and the melt matrix (optical microscope, plane-polarized light and SEM-BSE image, respectively). c) and d) Black, granular textured zircon grain embedded in the melt rock matrix (optical microscope, plane polarized light, and SEM-BSE image, respectively). Note that the granular texture exhibits abundant microvesicles and tiny inclusions of high mass contrast. e) and f) SEM-BSE images of zircon grain embedded in ballen quartz of annealed shock stage III gneiss fragment. The inclusion is apatite (ap).

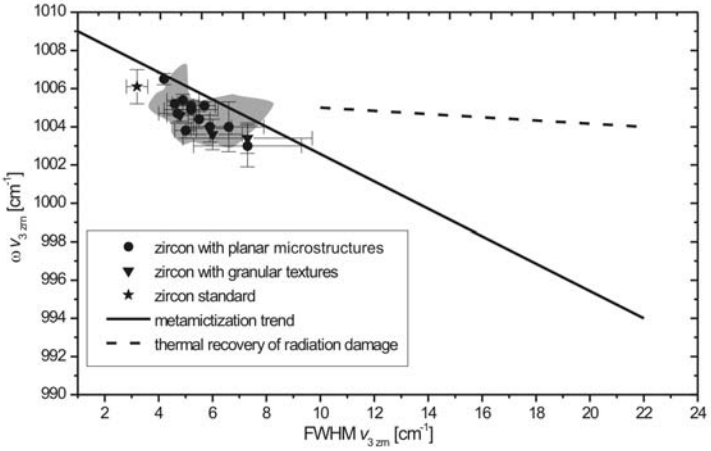

Fig. 11. Full width at half-maximum (FWHM) plotted versus Raman shift position of the v_3 anti-symmetric stretching mode of Si-O (ω v_3) in the Raman spectra of zircon grains from the Popigai impact melt rock samples. Error bars indicate standard deviation of a mean from multiple spectra of the same grain. For reference, means and standard deviation of 15 measurements of natural, unshocked zircon is plotted. The shaded area represents measurements of the zircons without shock features. Trend of radiation damage of zircon after Nasdala et al. (2002) and Geisler and Pidgeon (2002). Note that according to this trend, pronounced metamictization is indicated for FWHM >20 and ω v_3 < 1000. Thermal recovery trend after Geisler and Pidgeon (2002).

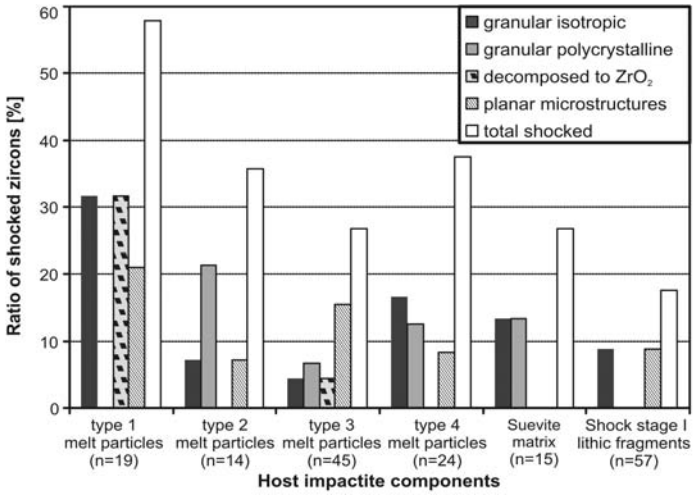

Fig. 12. The relative proportions of different shock effects in zircons of Yax-1 host components. Melt types after Hecht et al. (2004). All shocked grains in the lithic fragments of shock stage I occur in the fragment that experienced upper shock stage I conditions with an estimated shock pressure >20 GPa. Single grains can exhibit multiple shock features, therefore, ratios of all shock features do not generally add up to the ratio of total shocked grains.

experimentally shocked samples, or by Zhang et al. (2000b) from amorphous zircon coexisting with SiO_2 and tetragonal ZrO_2, were not consistently identified. However, we found systematic background intensity variations in Raman spectra of the experimentally shocked samples (Fig. 3). This pattern could indicate an increase in coexisting amorphous material in the samples from 38–60 GPa, which approximately span the mixed phase regime (Fig. 17). In the high-pressure phase regime at 80 GPa, background intensity drops towards the level of the unshocked, non-metamict precursor zircon.

Distinct steps of thermal recovery of amorphous zircon are known from annealing experiments between ~1100–1450 °C that result in distinct granular textures (Weber 1990; McLaren et al. 1994; Capitani et al. 2000; Zhang et al. 2000a; Ewing et al. 2003). Granular textured zircon with dark colors and reduced birefringence may therefore represent less intense thermal annealing at lower temperatures, while the polycrystalline type probably experienced more prolonged annealing at higher temperatures. Because diaplectic glasses can crystallize at far lower temperatures than "normal" glass (Dworak 1969; Rehfeldt-Oskierski et al. 1986; Stöffler and Langenhorst 1994), the thermal annealing of diaplectic zircon glass could occur at far lower temperatures than needed for the decomposition of zircon.

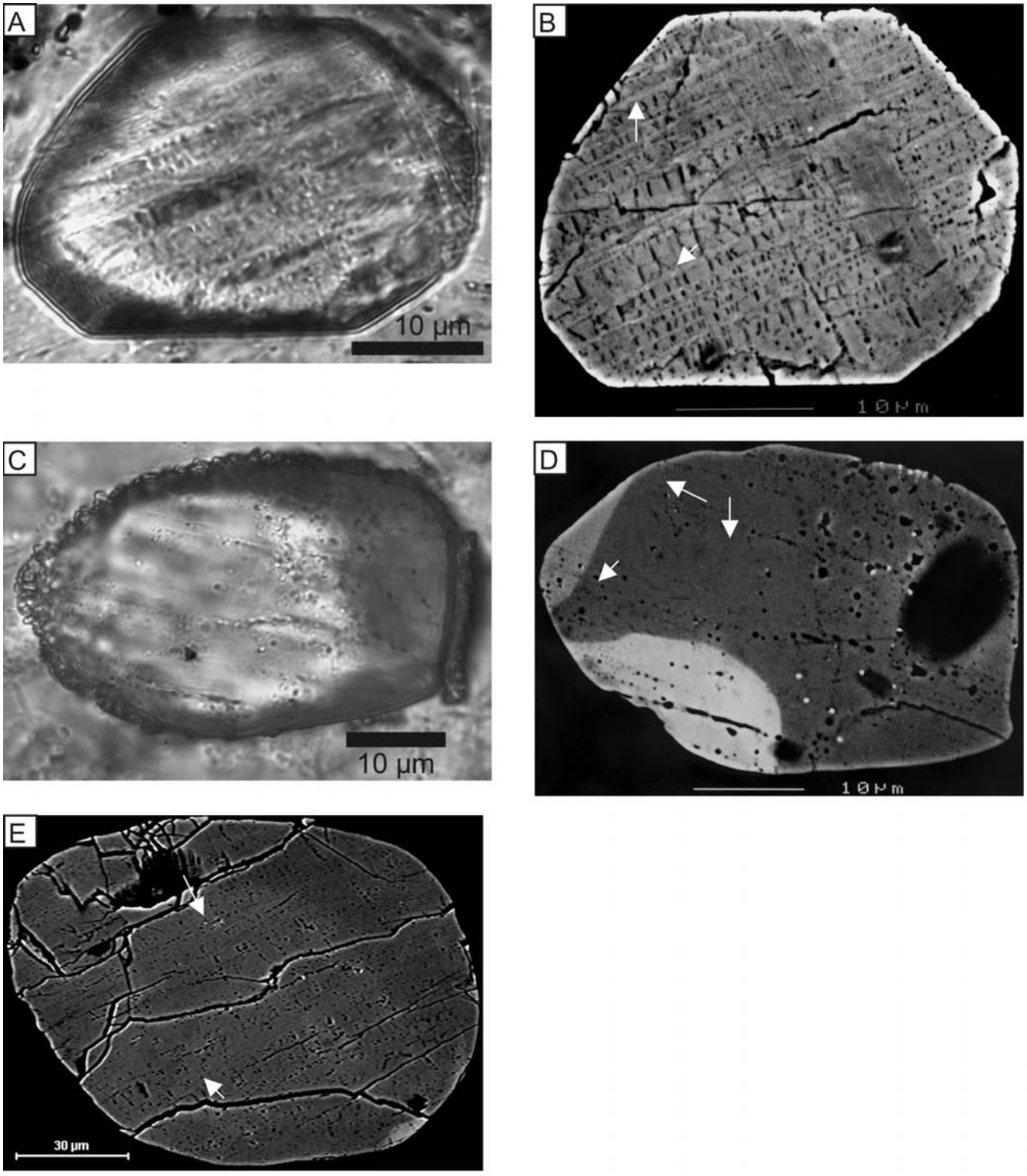

Fig. 13. a) and b) Euhedral zircon grain in type 2 melt rock host of SD sample at 916.65 m. Two bands of intersecting planar microstructures are present in the zircon grain (arrows) (optical microscope, plane-polarized light and SEM-BSE image, respectively). c) and d) Subhedral zircon grain in perlitic type 1 melt particle host in LSS sample at 818.51 m. One strongly and two additional weakly expressed parallel bands are displayed (arrows) (optical microscope, plane-polarized light and SEM-BSE image, respectively). e) Subhedral zircon grain with two sets of planar microstructures (arrows) in type 1 melt particle from SD sample at 916.60 m (SEM-BSE image).

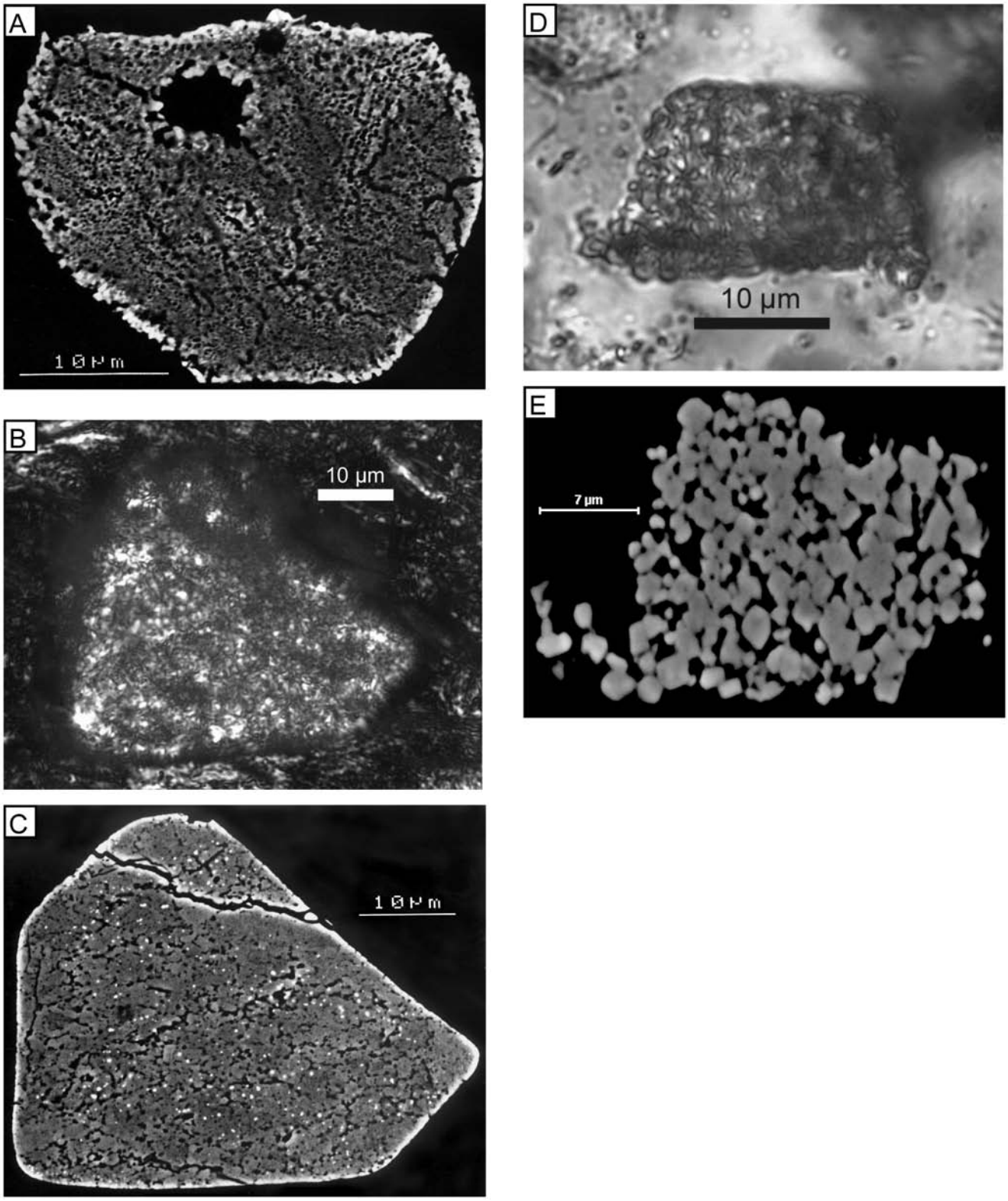

Fig. 14. a) Subhedral zircon grain with a granular texture that exhibits abundant microvesicles in the clastic matrix of US sample at 824.01 m (SEM-BSE image). b) and c) Polycrystalline, granular textured zircon grain of US sample at 824.01 m that is enclosed in a type 2 melt particle (optical microscope, crossed polarizers and SEM-BSE image, respectively). d) and e) Coarsely crystallized, composite zircon grain in blocky quartz of BMR sample at 875.35 m (optical microscope, crossed polarizers and SEM-BSE image, respectively).

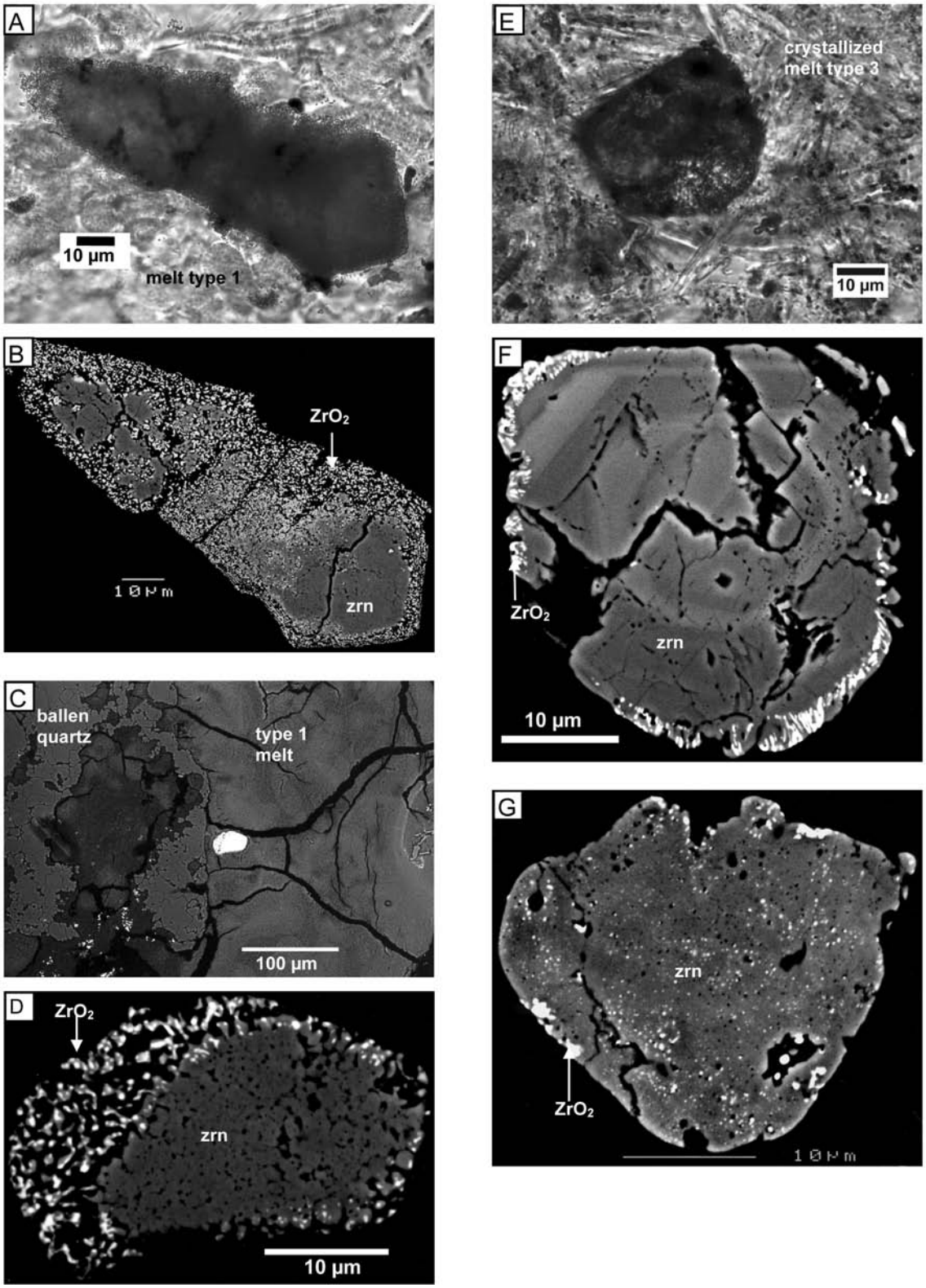

Fig. 15. a) and b) Decomposed zircon grain in USS sample at 800.25 m. Enclosed in a perlitic type 1 melt particle, it exhibits a granular texture and a rim of ZrO_2 granules (plane-polarized light and SEM-BSE image, respectively). c) and d) Decomposed zircon grain in US sample at 823.86 m. Embedded in a type 1 melt particle, it has a granular texture and rim of granular to vermicular ZrO_2-zircon intergrowths (SEM-BSE images). e) and f) Zircon grain enclosed in a type 3 melt particle in LS sample at 889.32 m with a rim of zircon-baddeleyite intergrowths and compositionally zoned core (plane-polarized light and SEM-BSE image, respectively). g) Granular textured zircon grain in a type 3 melt particle of SD sample at 916.23 m with baddeleyite patches (SEM-BSE image).

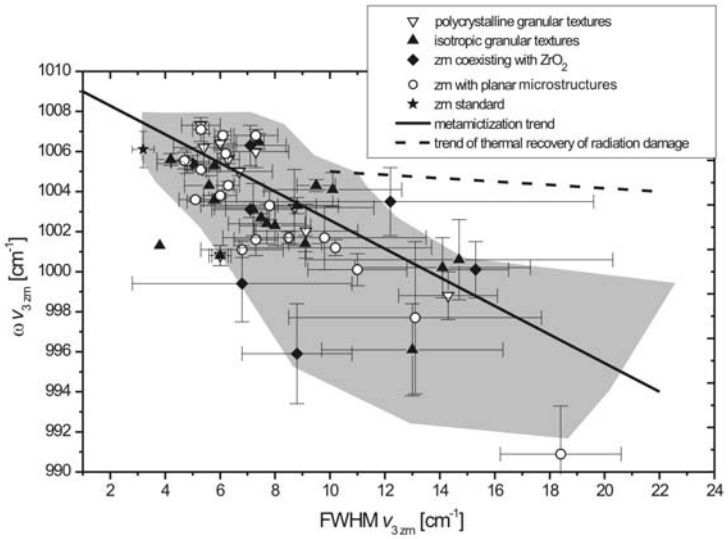

Fig. 16. Full width at half-maximum (FWHM) plotted versus Raman shift frequency (ω) of the ν_3 anti-symmetric stretching mode of Si-O in the Raman spectra of zircon grains in Yax-1 samples. Means of several measurements and standard deviations (error bars) are plotted. Shaded area represents measurements of Yax-1 zircons without shock features. Solid line marks trend of natural radiation damage of zircon after Nasdala et al. (2001) and Geisler and Pidgeon (2002). Dashed line represents thermal annealing trend of metamict zircon after Geisler and Pidgeon (2002).

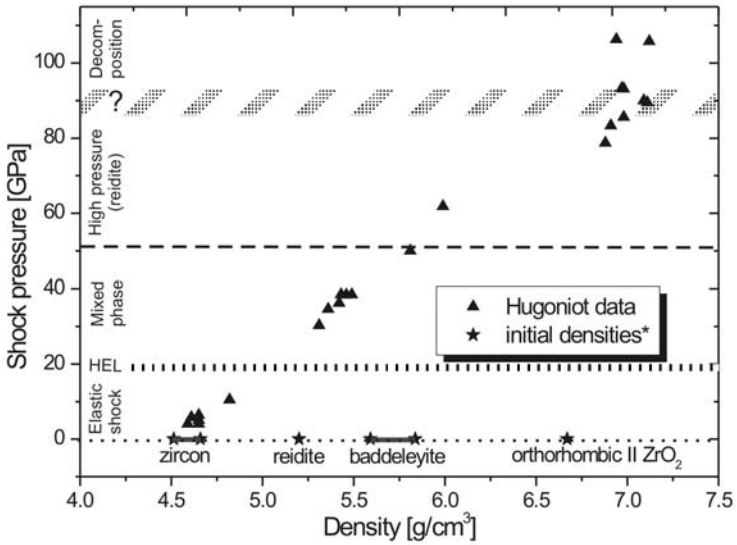

Fig. 17. Hugoniot data and ranges of initial densities for zircon and baddeleyite from Mashimo et al. (1983). Phase boundaries redrawn after Mashimo et al. (1983) and Fiske et al. (1994). Reidite density after Glass et al. (2002), density of orthorhombic II ZrO_2 after Liu (1979).

Implications for Yax-1

The full range of progressive stages of shock metamorphism was found to occur in crystalline basement clasts of all suevitic units in Yax-1 (Schmitt et al. 2003; Stöffler et al. 2004; Kring et al. 2004; Dressler et al. 2004; Tuchscherer et al. 2004a). However, all shock features in quartz and feldspar are annealed and melt components can be distinguished by variable degrees of devitrification before and during quenching. The principal results of this study indicate that perlitic type 1 melt particles are indicative of the most rapid quenching in Yax-1 (Fig. 1). This melt particle type is the dominant host for zircons that exhibit decomposition to ZrO_2. Also, all granular textured zircon grains found in this host are of the isotropized type that experienced least annealing. Moreover, this melt particle type retained the highest ratio of shocked versus unshocked zircon grains (Fig. 12). As shock stage IV materials, such melt particles indicate shock pressures >60 GPa and post-shock temperatures >1500 °C (Stöffler 1971a) (Fig. 18). Their

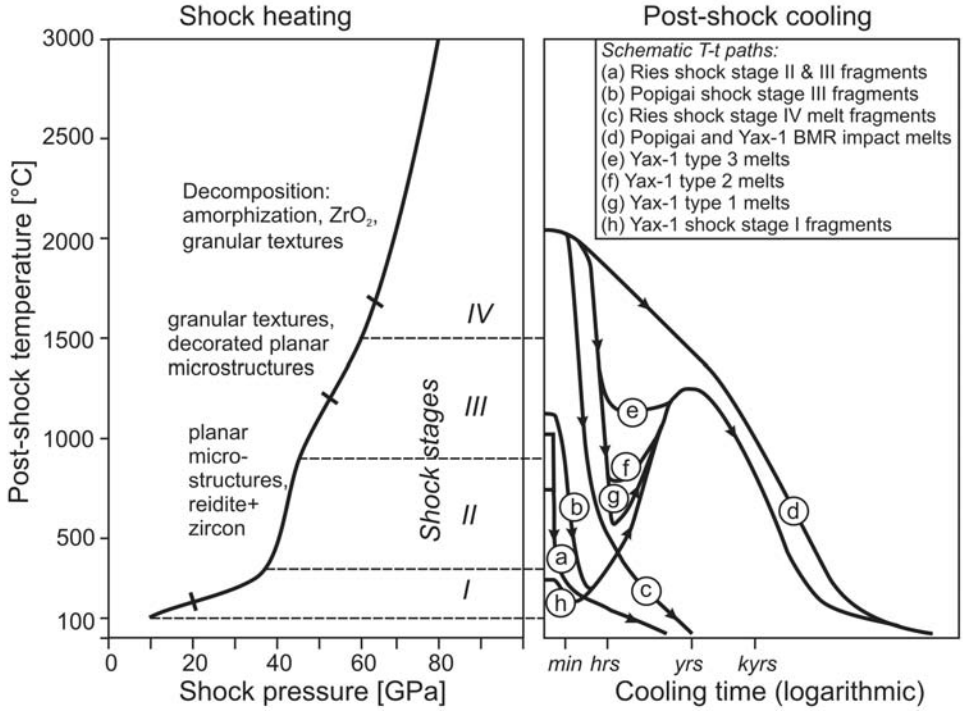

Fig. 18. Post-shock temperature as a function of shock pressure in naturally shocked, non-porous quartzo-feldspathic rocks (left) and respective shock stages after data from Stöffler (1971a). Stability ranges of shock features of $ZrSiO_4$ are projected into the diagram. Projections of schematic post-shock cooling paths for the naturally shocked samples analyzed in this study are plotted in the right diagram. Impact melt particle types of Yax-1 after Hecht et al. (2004).

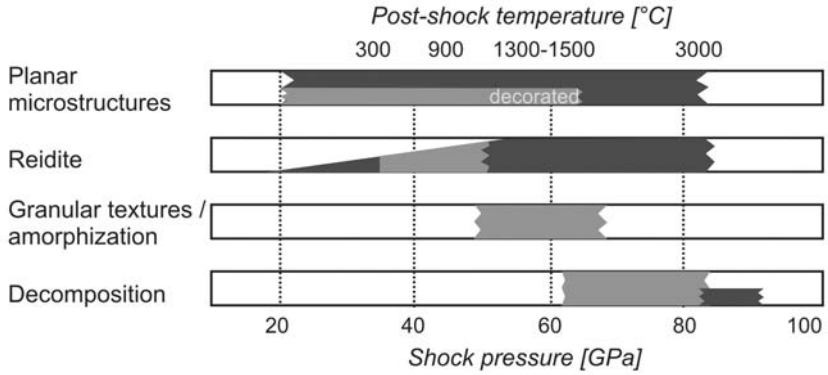

Fig. 19. A compilation of shock features of $ZrSiO_4$. Post-shock temperature estimates for non-porous quartzo-feldspathic rocks after Stöffler (1971a). Black shading indicates constraints from experimental evidence (Leroux et al. 1999; Mashimo et al. 1983; Fiske et al. 1994; Kusaba et al. 1985; this study). Grey shading indicates constraints from natural impactites.

cooling history allowed the crystallization of ballen quartz but the crystallization of liquidus phase phenocrysts was inhibited. This indicates rapid quenching below 600 °C from initial shock temperatures in excess of some 1500 °C, followed by thermal annealing to temperatures of about 1200 °C (Rehfeldt-Oskierski et al. 1986; Stöffler and Langenhorst 1994; von Engelhardt et al. 1995) (Fig. 18). Type 1 melt particles are restricted to the USS, LSS, the uppermost Upper Suevite (US), and the Suevitic Dike (SD) suevite units in Yax-1 (Fig. 1). Towards the BMR, decomposition textures of zircon become annealed and granular textured grains exhibit gradual coarsening and recovery of optical properties. This indicates an annealing gradient in Yax-1 with the highest quenching rates in the USS and the SD from temperatures >1676 °C (Butterman and Foster 1967) to below the glass transition temperature of melt particles of ~680 °C before deposition (Arndt and Häberle 1973; von Engelhardt et al. 1995). Quenching was slowest in the BMR because the temperature at which precipitation of liquidus phase phenocrysts ceases (~600 °C) (von Engelhardt et al. 1995)

had only been reached after abundant crystallization of liquidus phase phenocrysts had occurred (*T-t* path [d] in Fig. 18). This possibly allowed resorption of components in the BMR and development of reaction coronas around lithic fragments, similar to the Popigai impact melt rocks (Vishnevsky and Montanari 1999; Whitehead et al. 2002). General post-shock temperatures in excess of 1200 °C for the whole sequence are indicated by the lack of reidite, which is in accordance with the observations related to annealed shock features in quartz (Rehfeldt-Oskierski et al. 1986; Stöffler and Langenhorst 1994; Schmitt et al. 2003) (Fig. 18).

CONCLUSIONS

We combined our findings and experimental evidence for the occurrence of shock features in $ZrSiO_4$ in a diagram, which depicts the progressive stages of shock metamorphism of zircon (Fig. 19). A comparison of experimentally shocked zircon with zircons of rapidly quenched impactites from the Ries crater indicates that the martensitic transformation to the high-pressure polymorph reidite may be hampered by impurities and pre-impact metamictization. Therefore, compared to shock experiments, the martensitic transformation is far less extensive in samples shocked to comparable shock-pressures at the Ries crater. Nonetheless, natural reidite-zircon intergrowths occur in shock stage II and III gneiss fragments of the Ries suevite together with diaplectic quartz glass, coesite, and impact diamonds. Reidite can also occur very rarely incorporated in rapidly quenched shock stage IV impact melts of the suevite. Reidite-zircon grains of shock stage III fragments from the Ries crater show the onset of shock-induced amorphization but do not exhibit decomposition to ZrO_2. Paragenetic relationships with ballen quartz imply that reidite decomposes to granular textured zircon at temperatures >1100 °C. Granular textures in zircon do not occur in experimentally shocked zircon up to pressures of 80 GPa but were found as the most common impact-induced feature in the samples from the Chicxulub crater. We suggest that they represent the recovery from amorphized zircon in analogy to annealing textures of thermally recovered metamict zircon and reconverted zircon-reidite and reidite grains that were formed in a shock pressure range between 20 and >80 GPa. The development of this feature appears mainly due to high temperature annealing. Planar microstructures occur in experimentally shocked zircon with increasing abundance up to shock pressures of 80 GPa and seem to be linked to the martensitic transformation to reidite.

Decomposed zircon is restricted to shock stage IV impact melt particles. The low-temperature and low-pressure ZrO_2 polymorph baddeleyite is generally present in decomposed zircon, although it is not a stable high-temperature or high-pressure polymorph. We found possible relics of an orthorhombic II high-pressure polymorph of ZrO_2 that is the only quenchable high pressure polymorph of ZrO_2. The decomposition texture of zircon was not found in samples of impact melt rocks from the Popigai and Chicxulub craters that indicate extensive crystallization of phenocrysts. A systematic study of zircons in a continuous impactite deposit at the Chicxulub crater suggests annealing of decomposed zircon, PDFs and amorphous zircon. Shock features in zircon at Yax-1 reflect the cooling history of impact melt components until the cessation of phenocryst crystallization. This spans the time between formation of the impact melt until deposition and cooling below temperatures of ~600–680 °C.

Acknowledgments–This study received funding from the German Science Foundation grant KE 732-8. Wolf Uwe Reimold (Humboldt-Universität zu Berlin), Christian Koeberl (Universität Wien) and Ulrich Hornemann (Ernst-Mach Institut) are thanked for providing the experimentally shocked samples. Roald Tagle (Vrije Universiteit Brussel) spurred further interest and provided the Popigai samples. Richard Grieve gave valuable suggestions that improved the manuscript. Arnold Gucsik (University of West Hungary) sparked insightful discussions. We are further indebted to the staff at the Department of Mineralogy for their continuous support: Lutz Hecht, Ansgar Greshake, Jörg Fritz, Tobias Salge, Daniel Doman, Frank Schönian, Hwa Ja Nier, Rudolf Knöfler, Peter Czaja, Irmgard Felber, and Matthias Siebenschock. We are grateful for the concise suggestions of J. Spray, D. Davies and an anonymous reviewer. This paper is part of A. Wittmann's Ph.D. thesis.

Editorial Handling—Dr. John Spray

REFERENCES

Arashi H., Yagi T., Akimoto S., and Kudoh Y. 1990. New high-pressure phase of ZrO_2 above 35 GPa. *Physical Review B* 41: 4309–4313.

Arndt J. and Häberle F. 1973. Thermal expansion and glass transition temperatures of synthetic glasses of plagioclase-H-like compositions. *Contributions to Mineralogy and Petrology* 39: 175–183.

Bohor B. F., Betterton W. J., and Krogh T. E. 1993. Impact-shocked zircons: Discovery of shock-induced textures reflecting increasing degrees of shock metamorphism. *Earth and Planetary Science Letters* 119:419–424.

Bottomley R., Grieve R., York D., and Masaitis V. 1997. The age of the Popigai impact event and its relation to events at the Eocene/Oligocene boundary. *Nature* 388:365–368.

Butterman W. C. and Foster W. R. 1967. Zircon stability and the ZrO_2-SiO2 phase diagram. *American Mineralogist* 52:880–885.

Capitani G. C., Leroux L., Doukhan J. C., Ríos S., Zhang M., and Salje E. K. H. 2000. A TEM investigation of natural metamict zircons: Structure and recovery of amorphous domains. *Physics and Chemistry of Minerals* 27:545–556.

Corfu F., Hanchar J. M., Hoskin P. W. O., and Kinny P. 2003. Atlas of zircon textures. In *Zircon*, edited by Hanchar J. M. and Hoskin P. W. O. Washington, D.C.: Mineralogical Society of America. pp. 469–500.

DeCarli P. S., Bowden E., Jones A. P., and Price G. D. 2002. Laboratory impact experiments versus natural impact events. In *Catastrophic events and mass extinctions: Impacts and beyond*, edited by Koeberl C. and MacLeod K. G. Boulder, Colorado: Geological Society of America. pp. 595–605.

Deloule E., Chaudisson M., Glass B. P., and Koeberl C. 2001. U-Pb isotopic study of relict zircon inclusions recovered from Muong Nong-type tektites. *Geochimica et Cosmochimica Acta* 65: 1833–1838.

Deutsch A. and Schärer U. 1990. Isotope systematics and shock-wave metamorphism: I. U-Pb in zircon, titanite and monazite, shocked experimentally up to 59 GPa. *Geochimica et Cosmochimica Acta* 54:3427–3434.

Dobretsov N. L., Dobretsova I. L., Sobolev V. S., and Mali V. I. 1969. Shock compression of $ZrSiO_4$ and metamict decay. *Doklady Akademii Nauk USSR* 182:134–137.

Dressler B. O., Sharpton V. L., Morgan J., Buffler R., Moran D., Smit J., Stöffler D., and Urrutia J. 2003. Investigating a 65-Ma-old smoking gun: Deep drilling of the Chicxulub impact structure. *EOS Transactions* 84:125–130.

Dressler B. O., Sharpton V. L., Schwandt C. S., and Ames D. 2004. Impactites of the Yaxcopoil-1 drilling site, Chicxulub impact structure: Petrography, geochemistry, and depositional environment. *Meteoritics & Planetary Science* 39:857–878.

Dworak U. 1969. Stosswellenmetamorphose des Anorthosites vom Manicouagan Krater, Quebec, Canada. *Contributions to Mineralogy and Petrology* 24:306–347.

El Goresy A. 1965. Baddeleyite and its significance in impact glasses. *Journal of Geophysical Research* 70:3453–3456.

El Goresy A. 1968. The opaque minerals in impactite glasses. In *Shock metamorphism of natural materials*, edited by French B. W. and Short N. M. Baltimore, Maryland: Mono Book Corp. pp. 531–553.

El Goresy A., Gillet P., Chen M., Künstler F., Graup G., and Stähle V. 2001a. In situ discovery of shock-induced graphite-diamond phase transition in gneisses from the Ries crater, Germany. *American Mineralogist* 86:611–621.

El Goresy A., Chen M., Dubrovinsky L., Gillet P., and Graup G. 2001b. An ultradense polymorph of rutile with seven-coordinated titanium from the Ries crater. *Science* 293:1467–1470.

El Goresy A., Dubrovinsky L. S., Gillet P., Mostefaoui S., Graup G., Drakopoulos M., Simionovici A. S., Swamy Y., and Masaitis V. L. 2003. A novel cubic, transparent and super-hard polymorph of carbon from the Ries and Popigai craters: Implications to understanding dynamic-induced natural high-pressure phase transitions in the carbon system (abstract # 1016). 34th Lunar and Planetary Science Conference. CD-ROM.

Ewing R. C., Meldrum A., Wang L., Weber W. J., and Corrales L. R. 2003. Radiation effects in zircon. In *Zircon*, edited by Hanchar J. M. and Hoskin P. W. O. Washington, D.C.: Mineralogical Society of America. pp. 387–425.

Finch R. J. and Hanchar J. M. 2003. Structure and chemistry of zircon and zircon-group minerals. In *Zircon*, edited by Hanchar J. M. and Hoskin P. W. O. Washington, D.C.: Mineralogical Society of America. pp. 1–25.

Fiske P. S., Nellis W. J., and Sinha A. K. 1994. Shock-induced phase transitions of $ZrSiO_4$, reversion kinetics, and implications for terrestrial impact craters (abstract). *EOS Transactions* 75:416–417.

Geisler T. and Pidgeon R. T. 2002. Raman scattering from metamict zircon: Comments on "Metamictisation of natural zircon: Accumulation versus thermal annealing of radioactivity-induced damage." *Contributions to Mineralogy and Petrology* 143:750–755.

Gibson R. L., Armstrong R. A., and Reimold W. U. 1997. The age and thermal evolution of the Vredefort impact structure: A single-grain U-Pb zircon study. *Geochimica et Cosmochimica Acta* 61:1531–1540.

Glass B. P., Wasson J. T., and Futrell D. S. 1990. A layered moldavite containing baddeleyite. Proceedings, 20th Lunar and Planetary Science Conference. pp. 415–420.

Glass B. P., Koeberl C., Blum J. D., Senftle F., Izett G. A., Evans B. J., Thorpe A. N., Povenmire H., and Strange R. L. 1995. A Muong Nong-type Georgia tektite. *Geochimica et Cosmochimica Acta* 59:4071–4082.

Glass B. P., Wasson J. T., and Futrell D. S. 2000. Relict zircon inclusions in Muong Nong-type Australasian tektites: Implications regarding the location of the source crater (abstract). 31st Lunar and Planetary Science Conference. CD-ROM.

Glass B. P. and Liu S. 2001. Discovery of high-pressure $ZrSiO_4$ polymorph in naturally occurring shock-metamorphosed zircons. *Geology* 29:371–373.

Glass B. P., Liu S., and Leavens P. 2002. Reidite: An impact-produced high-pressure polymorph of zircon in marine sediments. *American Mineralogist* 87:562–565.

Grieve R. A. F., Langenhorst F., and Stöffler D. 1996. Shock metamorphism of quartz in nature and experiment: II. Significance in geoscience. *Meteoritics & Planetary Science* 31: 6–35.

Gucsik A., Koeberl C., Brandstätter F., Libowitzky E., and Reimold W. U. 2004a. Cathodoluminescence, electron microscopy, and Raman spectroscopy of experimentally shock metamorphosed zircon crystals and naturally shocked zircon from the Ries impact crater. In *Cratering in marine environments and on ice*, edited by Dypvik H., Claeys P., and Burchell M. Heidelberg: Springer. pp. 281–322.

Gucsik A., Zhang M., Koeberl C., Salje E. K. H., Redfern S. A. T., and Pruneda J. M. 2004b. Infrared and Raman spectra of $ZrSiO_4$ experimentally shocked at high pressures. *Mineralogical Magazine* 68:801–811.

Haines J., Léger J. M., Hull S., Petitet J. P., Pereira A. S., Perottoni C. A., and da Jornada J. O. H. 1997. Characterization of the cotunnite-type phases of zirconia and hafnia by neutron diffraction and Raman spectroscopy. *Journal of the American Ceramic Society* 80:1910–1914.

Hecht L., Wittmann A., Schmitt R. T., and Stöffler D. 2004. Composition of impact melt particles and the effects of post-impact alteration in suevitic rocks at the YAX-1 drill core, Chicxulub crater, Mexico. *Meteoritics & Planetary Science* 39: 1169–1186.

Heider N. and Kenkmann T. 2003. Numerical simulations of temperature effects at fissures due to shock loading. *Meteoritics & Planetary Science* 39:1451–1460.

Hildebrand A. R., Penfield G. T., Kring D. A., Pilkington M., Camargo Zanoguera A., and Jacobsen S. B. 1991. Chicxulub crater: A possible Cretaceous/Tertiary boundary impact crater on the Yucatán Peninsula, Mexico. *Geology* 19:867–871.

Hildebrand A. R., Pilkington M., Connors M., Ortiz-Aleman C., and Chavez R. E. 1995. Size and structure of the Chicxulub crater revealed by horizontal gravity gradients and cenotes. *Nature* 376: 415–417.

Hough R. M., Gilmour I., Pillinger C. T., Arden J. W., Gilkes K. W. R., Yuan J., and Milledge H. J. 1995. Diamond and silicon carbide in impact melt rock from the Ries impact crater. *Nature* 378:41–44.

Hörz F. 1965. Untersuchungen an Riesgläsern. *Beiträge zur Mineralogie & Petrographie* 11:621–661.

Kamo S. L., Reimold W. U., Krogh T. E., and Colliston W. P. 1996.

A 2.023 Ga age for the Vredefort impact event and a first report of shock metamorphosed zircons in pseudotachylitic breccias and granophyre. *Earth and Planetary Science Letters* 144:369–387.

Kenkmann T., Wittmann A., and Scherler D. 2004. Structure and impact indicators of the Cretaceous sequence of the ICDP drill core Yaxcopoil-1, Chicxulub impact crater, Mexico. *Meteoritics & Planetary Science* 39:1069–1088.

Kleinmann B. 1969. The breakdown of zircon observed in the Libyan desert glass as evidence of its impact origin. *Earth and Planetary Science Letters* 5:497–501.

Knittle E. and Williams Q. 1993. High-pressure Raman spectroscopy of $ZrSiO_4$: Observation of the zircon to scheelite transition at 300 K. *American Mineralogist* 78:245–252.

Koeberl C. and Reimold W. U. 2003. Geochemistry and petrography of impact breccias and target rocks from the 145 Ma Morokweng impact structure, South Africa. *Geochimica et Cosmochimica Acta* 67:1837–1862.

Kring D. A., Hörz F., and Zürcher L. 2004. Impact lithologies and their emplacement in the Chicxulub impact crater: Initial results from the Chicxulub Scientific Drilling Project, Yaxcopoil, Mexico. *Meteoritics & Planetary Science* 39:879–898.

Krogh T. E. and Davis D. W. 1984. Morphological and isotopic similarities between shocked (?) Archean zircons in the Levack Gneiss and Onaping formations (abstract). Geological Association of Canada program with abstracts. p. 79.

Krogh T. E., Kamo S. L., and Bohor B. F. 1993a. Fingerprinting the K/T impact site and determining the time of impact by U-Pb dating of single shocked zircons from distal ejecta. *Earth and Planetary Science Letters* 119:425–429.

Krogh T. E., Kamo S. L., Sharpton V. L., Marin L. E., and Hildebrand A. R. 1993b. U-Pb ages of single shocked zircons linking distal K/T ejecta to the Chicxulub crater. *Nature* 366:731–734.

Krogh T. E., Kamo S. L., and Bohor B. F. 1996. Shock metamorphosed zircons with correlated U-Pb discordance and melt rocks with concordant protolith ages indicate an impact origin for the Sudbury structure. In *Earth processes: Reading the isotopic code*, edited by Hart S. and Basu A. Washington, D.C.: American Geophysical Union. 437 p.

Kusaba K., Syono Y., Kikuchi M., and Fukuoka K. 1985. Shock behaviour of zircon: Phase transitions to scheelite structure and decomposition. *Earth and Planetary Science Letters* 72:433–439.

Kusaba K., Yagi T., Kikuchi M., and Syono Y. 1986. Structural considerations on the mechanism of the shock-induced zircon-scheelite transition in $ZrSiO_4$. *Journal of Physics and Chemistry of Solids* 47:675–679.

Laurenzi M. A., Bigazzi G., Balestrieri M. L., and Bouska V. 2003. $^{40}Ar/^{39}Ar$ laser probe dating of the Central European tektite-producing impact event. *Meteoritics & Planetary Science* 38: 887–893.

Leroux H. and Doukhan J.-C. 1996. A transmission electron microscope study of shocked quartz from the Manson impact structure. In *The Manson impact structure, Iowa: Anatomy of an impact crater*, edited by Koeberl C. and Anderson C. C. Boulder, Colorado: Geological Society of America. pp. 267–274.

Leroux H., Reimold W. U., Koeberl C., Hornemann U., and Doukhan J.-C. 1999. Experimental shock deformation in zircon: A transmission electron microscopic study. *Earth and Planetary Science Letters* 169:291–301.

Liu L.-G. 1979. High-pressure phase transformations in baddeleyite and zircon, with geophysical implications. *Earth and Planetary Science Letters* 44:390–396.

López E. F., Escribano V. S., Panizza M., Carnasciali M., and Busca G. 2001. Vibrational and electronic spectroscopic properties of zirconia powders. *Journal of Materials Chemistry* 11:1891–1897.

López Ramos E. 1975. Geologic summary of the Yucatán Peninsula. In *The ocean basins and margins, volume 3: The Gulf of Mexico and the Caribbean*, edited by Nairn A. E. M. and Stehli F. G. New York: Plenum Press. pp. 257–282.

Marvin U. B. and Kring D. A. 1992. Authentication controversies and impactite petrography of the New Quebec crater. *Meteoritics & Planetary Science* 27:585–595.

Masaitis V. L. 1994. Impactites from Popigai crater. In *Large meteorite impacts and planetary evolution*, edited by Dressler B. O. Boulder, Colorado: Geological Society of America. pp. 153–162.

Mashimo T., Nagayama K., and Sawaoka A. 1983. Shock compression of zirconia ZrO_2 and zircon $ZrSiO_4$ in the pressure range up to 150 GPa. *Physics and Chemistry of Minerals* 9:237–247.

McLaren A. C., Fitzgerald J. D., and Williams I. S. 1994. The microstructure of zircon and its influence on the age determination from Pb/U isotopic rations measured by ion microprobe. *Geochimica et Cosmochimica Acta* 58:993–1005.

Morgan J., Warner M., Brittan J., Buffler R., Camargo A., Christeson G., Denton P., Hildebrand A., Hobbs R., MacIntyre H., MacKenzie G., Maguire P., Marin L., Nakamura Y., Pilkington M., Sharpton V., Snyder D., Suarez G., and Trejo A. 1997. Size and morphology of the Chicxulub impact crater. *Nature* 390:472–476.

Morgan J. V., Warner M. R., Collins G. S., Melosh H. J., and Christeson G. L. 2000. Peak-ring formation in large impact craters: geophysical constraints from Chicxulub. *Earth and Planetary Science Letters* 183:347–354.

Nasdala L., Irmer G., and Wolf D. 1995. The degree of metamictization in zircon: A Raman spectroscopic study. *European Journal of Mineralogy* 7:471–478.

Nasdala L. M. W., Vavra G., Irmer G., Wenzel T., and Kober B. 2001. Metamictization of natural zircon: Accumulation versus thermal annealing of radioactivity-induced damage. *Contributions to Mineralogy and Petrology* 141:125–144.

Nasdala L., Lengauer C. L., Hanchar J. M., Kronz A., Wirth R., Blanc P., Kennedy A. K., and Seydoux-Guillaume A.-M. 2002. Annealing radiation damage and the recovery of cathodoluminescence. *Chemical Geology* 191:121–140.

Nasdala L., Reiners P. W., Garver J. I., Kennedy A. K., Stern R. A., Balan E., and Wirth R. 2004. Incomplete retention of radiation damage in zircon from Sri Lanka. *American Mineralogist* 89: 219–231.

Newsom H. E., Graup G., Iseri D. A., Geissman J. W., and Keil K. 1990. The formation of the Ries crater, West Germany: Evidence of atmospheric interactions during a larger cratering event. In *Global catastrophes in Earth history*, edited by Sharpton V. L. and Ward P. D. Boulder, Colorado: Geological Society of America. pp. 195–206.

Ohtaka O., Yamanaka T., and Yagi T. 1994. New high-pressure and temperature phase of ZrO_2 above 1000 °C at 20 GPa. *Physical Review B* 49:9295–9298.

Osinski G. R. 2003. Impact glasses in fallout suevites from the Ries impact structure, Germany: An analytical SEM study. *Meteoritics & Planetary Science* 38:1641–1667.

Rehfeldt-Oskierski A., Stöffler D., and Hornemann U. 1986. Deformation, transformation, and thermal annealing of experimentally shocked single crystal quartz (abstract). 17th Lunar and Planetary Science Conference. pp. 697–698.

Reid A. F. and Ringwood A. E. 1969. Newly observed high pressure transformations in Mn_3O_4, $CaAl_2O_4$, and $ZrSiO_4$. *Earth and Planetary Science Letters* 6:205–208.

Reimold W. U., Leroux H., and Gibson R. L. 2002. Shocked and thermally metamorphosed zircon from the Vredefort impact structure, South Africa: A transmission electron microscopic study. *European Journal of Mineralogy* 14:859–868.

Schmitt R. T., Wittmann A., and Stöffler D. 2003. The ICDP drill core Yaxcopoil-1, Chicxulub impact crater, Mexico: Shock metamorphism of the impactite units (794–894 m) (abstract #4061). 3rd Conference on Large Meteorite Impacts. CD-ROM.

Schmitt R. T., Lapke C., Lingemann C., Siebenschock M., and Stöffler D. 2005. Distribution and origin of impact diamonds in the Ries crater, Germany. In *Large meteorite impacts III*, edited by Kenkmann T., Hörz F., and Deutsch A. Boulder, Colorado: Geological Society of America. pp. 299–314.

Short N. M. 1970. Progressive shock metamorphism of quartzite ejecta from the Sedan nuclear explosion crater. *Journal of Geology* 78:705–723.

Stöffler D. 1971a. Progressive metamorphism and classification of shocked and brecciated crystalline rocks at impact craters. *Journal of Geophysical Research* 76:5541–5551.

Stöffler D. 1971b. Coesite and stishovite in shocked crystalline rocks. *Journal of Geophysical Research* 76:5474–5488.

Stöffler D. 1972. Deformation and transformation of rock-forming minerals by natural and experimental shock processes. I. Behaviour of minerals under shock compression. *Fortschritte der Mineralogie* 49:50–113.

Stöffler D. 1974a. Cratering mechanics, impact metamorphism and distribution of ejected masses of the Ries structure—An introduction. *Fortschritte der Mineralogie* 52:103–122.

Stöffler D. 1974b. Deformation and transformation of rock-forming minerals by natural and experimental shock processes. II. Physical properties of shocked minerals. F*ortschritte der Mineralogie* 51:256–289.

Stöffler D. and Ostertag R. 1983. The Ries impact crater. *Fortschritte der Mineralogie* 61:71–116.

Stöffler D. and Langenhorst F. 1994. Shock metamorphism of quartz in nature and experiment: I. Basic observation and theory. *Meteoritics* 29:155–181.

Stöffler D., Artemieva N. A., Ivanov B. A., Hecht L., Kenkmann T., Schmitt R. T., Tagle R. A., and Wittmann A. 2004. Origin and emplacement of the impact formations at Chicxulub, Mexico, as revealed by the ICDP deep drilling Yaxcopoil-1 and by numerical modeling. *Meteoritics & Planetary Science* 39:1035–1068.

Swisher C. C. I., Grajales-Nishimura J. M., Montanari A., Margolis S. V., Claeys P., Alvarez W., Renne P., Cedillo-Pardo E., Maurasse F. J.-M. R., Curtis G. H., Smit J., and McWilliams M. O. 1992. Coeval $^{40}Ar/^{39}Ar$ ages of 65.0 million years ago from Chicxulub melt rock and Cretaceous-Tertiary boundary tektites. *Science* 257:954–958.

Tuchscherer M. G., Reimold W. U., Koeberl C., Gibson R. L., and de Bruin D. 2004a. First petrographic results on impactites from the Yaxcopoil-1 borehole, Chicxulub structure, Mexico. *Meteoritics & Planetary Science* 39:899–930.

Tuchscherer M. G., Reimold W. U., Koeberl C., and Gibson R. L. 2004b. Major and trace element characteristics of impactites from the Yaxcopoil-1 borehole, Chicxulub structure, Mexico. *Meteoritics & Planetary Science* 39:955–978.

Urrutia-Fucugauchi J., Morgan J., Stöffler D., and Claeys P. 2004. The Chicxulub Scientific Drilling Project (CSDP). *Meteoritics & Planetary Science* 39:787–790.

van Westrenen W., Frank M. R., Hanchar J. M., Fei Y., Finch R. J., and Zha C.-S. 2004. In situ determination of the compressibility of synthetic pure zircon ($ZrSiO_4$) and the onset of the zircon-reidite phase transition. *American Mineralogist* 89:197–203.

Vermeesch P. M. and Morgan J. V. 2004. Chicxulub central crater structure: Initial results from physical property measurements and combined velocity and gravity modeling. *Meteoritics & Planetary Science* 39:1019–1034.

Vishnevsky S. and Montanari A. 1999. Popigai impact structure (Arctic Siberia, Russia): Geology, petrology, geochemistry, and geochronology of glass-bearing impactites. In *Large meteorite impacts and planetary evolution II*, edited by Dressler B. O. and Sharpton V. L. Boulder, Colorado: Geological Society of America. pp. 19–59.

von Engelhardt W., Stöffler D., and Schneider W. 1969. Petrologische Untersuchungen im Ries. *Geologica Bavarica* 61: 229–295.

von Engelhardt W. 1990. Distribution, petrography and shock metamorphism of the ejecta of the Ries crater in Germany—A review. *Tectonophysics* 171:259–273.

von Engelhardt W., Arndt J., Fecker B., and Pankau G. 1995. Suevite breccia from the Ries crater, Germany: Origin, cooling history and devitrification of impact glasses. *Meteoritics* 30:279–293.

von Engelhardt W. 1997. Suevite breccia of the Ries impact crater, Germany: Petrography, chemistry, and shock metamorphism of crystalline rock clasts. *Meteoritics & Planetary Science* 32:545–554.

Weber W. J. 1990. Radiation-induced defects and amorphization in zircon. *Journal of Materials Research* 5:2687–2697.

Whitehead J., Grieve R. A. F., and Spray J. G. 2002. Mineralogy and petrology of melt rocks from the Popigai impact structure, Siberia. *Meteoritics & Planetary Science* 37:623–647.

Wittmann A., Stöffler D., Schmitt R. T., Tagle R., Kenkmann T., and Hecht L. 2004a. Zircon as a shock indicator in impactites of drill core Yaxcopoil-1, Chicxulub impact structure, Mexico (abstract #1742). 35th Lunar and Planetary Science Conference. CD-ROM.

Wittmann A., Kenkmann T., Schmitt R. T., Hecht L., and Stöffler D. 2004b. Impact related dike breccia lithologies in the ICDP drill core Yaxcopoil-1, Chicxulub impact structure, Mexico. *Meteoritics & Planetary Science* 39:931–954.

Zhang M., Salje E. K. H., Ewing R. C., Farnan I., Ríos S., Schlüter J., and Leggo P. 2000a. Alpha-decay damage and recrystallization in zircon: Evidence for an intermediate state from infrared spectroscopy. *Journal of Physics: Condensed Matter* 12:5189–5199.

Zhang M., Salje E. K. H., Farnan I., Graeme-Barber A., Daniel P., Ewing R. C., Clark A. M., and Leroux H. 2000b. Metamictization of zircon: Raman spectroscopic study. *Journal of Physics: Condensed Matter* 12:1915–1925.